Studies of Ruthenium(II) Based Complexes Against Cancer

M.Sc. Thesis

By

SRESHTHA NAYEK

2003131025

DEPARTMENT OF CHEMISTRY

INDIAN INSTITUTE OF TECHNOLOGY INDORE

JUNE 2022

Studies of Ruthenium(II) Based Complexes Against Cancer

A THESIS

Submitted in partial fulfillment of the
Requirements for the award of the degree
of
Master of Science

by

SRESHTHA NAYEK

DEPARTMENT OF CHEMISTRY

INDIAN INSTITUTE OF TECHNOLOGY INDORE

JUNE 2022

INDIAN INSTITUTE OF TECHNOLOGY INDORE

CANDIDATE'S DECLARATION

I hereby certify that the work which is being presented in the thesis entitled **"Studies of Ruthenium(II) Based Complexes Against Cancer"** in the partial fulfillment of the requirements for the award of the degree of **MASTER OF SCIENCE** and submitted in the **DEPARTMENT OF CHEMISTRY, Indian Institute of Technology Indore**, is an authentic record of my own work carried out during the time period from **July 2021** to **June 2022** under the supervision of Dr. Suman Mukhopadhyay, Professor, Department of Chemistry, Indian Institute of Technology Indore.

The matter presented in this thesis has not been submitted by me for the award of any other degree of this or any other institute.

Sreshtha Nayek

SRESHTHA NAYEK

This is to certify that the above statement made by the candidate is correct to the best of my/our knowledge.

Dr. Suman Mukhopadhyay
Professor

SRESHTHA NAYEK has successfully given her M.Sc. Oral Examination held on 25/05/2022

Signature of Supervisor M.Sc. thesis
Date:

Tushar Kanti Mukherjee

Convenor, DPGC
Date: 27.05.2022

Signature of PSPC member 1
Date:

S. Sahoo

Signature of PSPC member 2
Date:

ACKNOWLEDGMENTS

This thesis would not have been possible without the support of many people who contributed in various ways for the successful completion of this project work.

First and foremost, I would like to express my deepest gratitude to my project supervisor **Prof. Suman Mukhopadhyay**. He introduced me to this fascinating subject through his enriching lectures which inspired me to take up this topic for my Masters project. I wish to thank him for his valuable guidance, his encouragement to keep moving forward and his motivating words to aim higher. His door was always open for offering any sort of advice and suggestions whenever needed. I feel very fortunate to have been under his guidance and am grateful for his dedicated support and consistent guidance throughout the course of this project.

I would like to extend my sincere thanks to my PSPC committee members **Prof. Apurba K. Das** and **Dr. Selvakumar Sermadurai** and DPGC convener **Dr. Tushar Kanti Mukherjee** for providing their insightful knowledge and suggestions. I also take this opportunity to thank our honorable Director **Prof. Suhas S. Joshi** and Head of the Chemistry Department, **Prof. Biswarup Pathak** for providing the infrastructure that was needed to carry out this project work. The entire faculty of IIT Indore and SIC persistently supported this project and I would like to acknowledge and thank their significant contribution as well.

I could not have undertaken this journey without the support of **Miss Pragti**, my mentor. Her valuable experience and knowledge of the field, continuous assistance and dedicated involvement in every step throughout the process from the very first day is what helped to make this research work possible and go as smoothly as possible. I am also thankful to other group members and friends who supported and helped me to the best of their abilities.

Throughout the year, the timely technical assistance provided by **Mr. Kinney Pandey**, **Mr. Ghanshyam Bhavsar**, and **Mr. Manish Kushwaha** is also greatly appreciated.

Finally, I will forever be grateful to my parents and sister for standing by me, showering me with unwavering love and support and encouraging me to keep exploring.

SRESHTHA NAYEK

Department of Chemistry

IIT Indore

DEDICATED TO ....

My beloved parents and sister for always supporting me in every way possible.

ABSTRACT

Recently in the field of chemotherapeutics to combat the side effects of cisplatin, ruthenium complexes are being investigated extensively. In this work, a bidentate benzimidazole based ligand, HL [HL=2-(1H-benzo[d]imidazol-2-yl)-6-methoxyphenol] was utilized to obtain three Ru(II) arene complexes having a generalized formula [Ru(η^6-p-cym)(L)(X)] (where p-cym = p-cymene, X = Cl) and [Ru(η^6-p-cym)(L)(X)]PF_6 (where p-cym = p-cymene, X = (i) PPh_3 = triphenyl phosphine, (ii) PTA = 1,3,5-triaza-7-phosphaadamantane) to explore their prospective anticancer activities. All of the synthesized compounds were characterized thoroughly using different analytical techniques including MS, NMR, FTIR, UV-Vis and fluorescence spectroscopy. A stability study using UV spectroscopy confirmed that the complexes remained stable in biological medium. It was also observed that both the ligand and the complexes are fluorescent in nature. A fluorescence quenching experiment with serum albumin proteins revealed that there is good interaction between the complexes and HSA (Human Serum Albumin) and BSA (Bovine Serum Albumin). The applications of the synthesized compounds were further explored by conducting a DNA binding study using absorption spectroscopy and fluorometric titration with DAPI (4',6-Diamidino-2-Phenylindole) to check whether the compound interacts with the DNA via groove binding. The complexes were additionally checked for their lipophilic nature and found to be catalyzing the transfer of hydrogen from NADH to get it converted into (Nicotinamide Adenine Dinucleotide) NAD^+, thus inducing oxidative stress. An MTT Assay revealed the extent of cytotoxicity of the compounds against different tumor cell lines. Furthermore, Hoechst staining indicated the ability of the complexes to bring about apoptosis in cancer cells.

TABLE OF CONTENTS

LIST OF FIGURES

LIST OF TABLES

NOMENCLATURE

Å	Angstrom
K_a	Binding Constant
cm	Centimeter
δ	Chemical Shift (NMR)
˚C	Degree Centigrade
τ	Fluorescence Lifetime
ν	Frequency
gm	Gram
K	Kelvin
L	Litre
µL	Micro Litre
µM	Micro Molar
mL	Milli Litre
mM	Milli Molar
mmol	Milli Mole
M	Molar
mol	Mole
nm	Nanometre
%	Percentage
K_{sv}	Stern Volmer Quenching Constant
λ	Wavelength

ACRONYMS

DAPI	4',6-Diamidino-2-Phenylindole
a.m.u	Atomic mass unit
BSA	Bovine Serum Albumin
C	Carbon
Cl	Chloride
DMF	Dimethylformamide
DMSO	Dimethylsulphoxide
ESI-MS	Electron Spray Ionisation-Mass Spectrometry
FT-IR	Fourier Transform- Infrared
HSA	Human Serum Albumin
HCl	Hydrochloric acid
H	Hydrogen
MeOH	Methanol
N	Nitrogen
NMR	Nuclear Magnetic Resonance
O	Oxygen
ppm	Parts per million
Pt	Platinum
KBr	Potassium Bromide
Ru	Ruthenium
Tris-HCl	Tris-Hydrochloric acid
UV	Ultraviolet
H_2O	Water

CHAPTER 1 Introduction

1.1 General Introduction

Cancer is a group of diseases that occurs when abnormal cells divide in an uncontrolled way and has the potential to invade other parts of the body**.** In 2018 itself, the number of new cases diagnosed were 18.1 million and 9.5 million patients were reported to have died due to the disease (Figure 1.1).[1] It is caused due to changes to genes that control our cell functions. Cancers can be broadly classified into carcinomas - derived from epithelial cells, sarcomas - originating from connective tissues, lymphoma and leukemia which is formed in the blood generating cells and blastoma arising from embryonic tissue.[2]

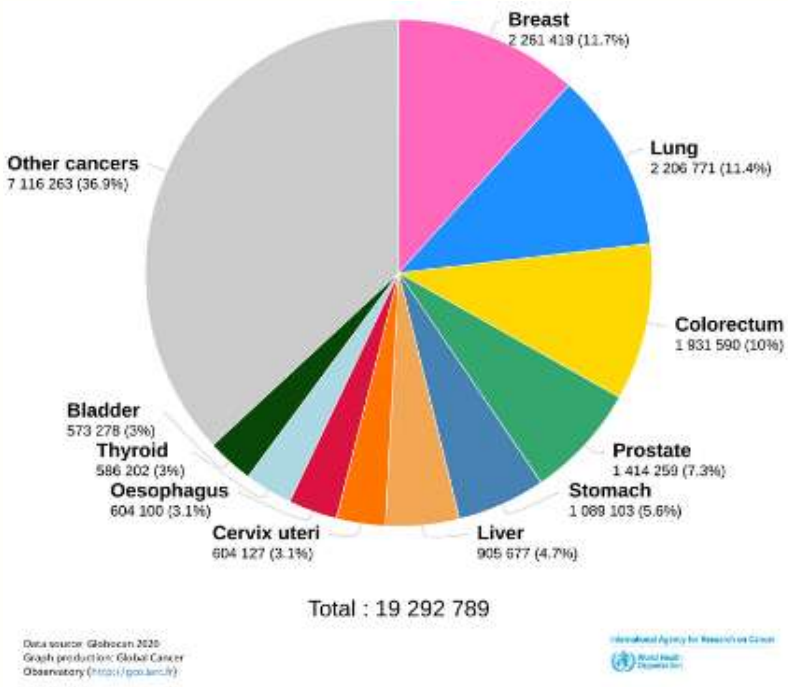

Figure 1.1*: Estimated number of new cases in 2020, worldwide.*

1.2 Metal Based Medicines and Cisplatin

Metals in trace amounts play a critical role in various metabolic functions in our bodies. They form components in the active sites of multiple enzymes and proteins and are actively involved in multiple biological processes like electron transfer reactions or the transportation of biological components across the body.[3] Throughout history of metallodrugs, metal containing medicines have been used to treat diseases like arthritis, diabetes, cardiovascular and gastrointestinal disorders and other microbial and viral diseases.[4] However, it is the accidental discovery of anticancer activity of cisplatin or cis-diamminedichloroplatinum(II) in the 1960s that sparked the interest towards metal based chemotherapeutics.

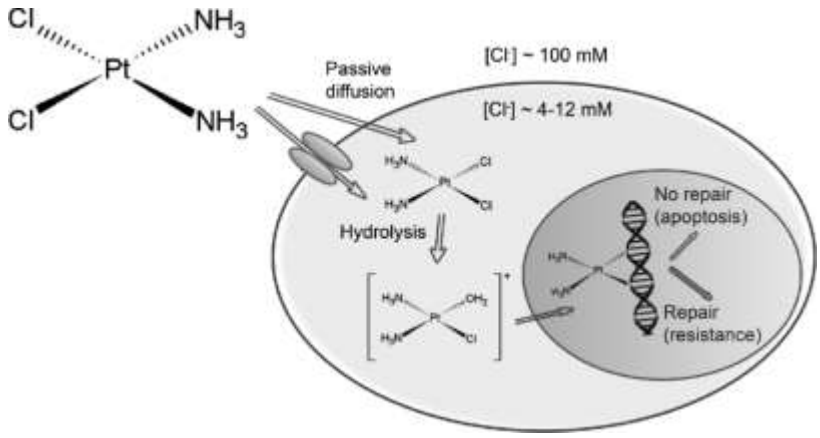

Figure 1.2*: Cisplatin and its mechanism of action.*

While being the most widely known, it is extremely effective to treat lung, bladder, head, neck and cervical cancers.[5–8] It is now extensively known that cisplatin binds to the DNA of the cell and causes hindrance to the process of DNA replication that ultimately leads to the termination of cell multiplication (Figure 1.2).[9] Unfortunately, cisplatin affects healthy cells as well as cancer cells, therefore causing side effects like kidney toxicity, nausea, vomiting.[10,11] For instance, nausea is caused because of inhibition of enzyme through coordination of Pt to sulfhydryl groups in protein. Apart from this, patients sometime develop tolerance to the drug after

repeated doses known as drug resistance, causing failure of treatment, thereby creating a need for alternative anticancer drugs.[12]

1.3 Ruthenium Anticancer Complexes

Thus in the pursuit of searching for a replacement, ruthenium complexes have emerged as an excellent replacement for platinum based metallodrugs in the field of chemotherapy due to a number of reasons. While Pt(II) can provide four coordination sites though a square planar geometry, six coordination sites of an octahedral ruthenium complex gives more flexibility in modulating the steric and electronic properties of the complex by introducing desired ligands. Importantly, Ru drugs also show a higher selectivity for cancer cells without affecting the healthy cells.[13] Rapidly multiplying cancer cells are in constant need of iron and hence transferrin receptors are over expressed. This observation combined with the property that Ru, by virtue of belonging to the same group as Fe, mimics it and thereby shows good binding with albumin proteins, results in an effective delivery of the drugs to the cancer cells.[14] A theory also speculates that if Ru drugs are administered in the +3 oxidation state which is the less reactive oxidised state, it will prove to be less harmful to the healthy cells. The complexes then get activated only in the tumor cells which tend to have a reducing atmosphere caused by a low oxygen concentration, high glutathione levels and acidic pH.[15] Ru(II) complexes and that of platinum(II) have similar ligand exchange rates of which is another reason for Ru to be considered as Pt alternative but with additional advantages.[16]

Cancer cells divide rapidly due to a loss of control of factors that are regulated by DNA. A lot of ruthenium compounds selectively bind to DNA as the metal atoms which are electron-deficient, act as acceptors of electron from the DNA moieties which act as nucleophiles. Moreover, unlike cisplatin, an advantage of Ru(II) complexes is that they can target

proteins other than targeting DNA in a cell.[17] Enzymes have important functions in various cellular processes like division of cells and apoptosis. Targeting any of these processes hinder normal cell function thus showing anticancer activity.

1.4 Ruthenium Arene Compounds

Half-sandwich arene ruthenium (II) complexes [(η^6-arene)Ru(X)(Y)(Z)] in particular, have attracted attention as promising candidates for anticancer activity (Figure 1.3). They are a class of compounds that have a piano stool geometry, where X and Y are either a bidentate ligand or two ligands that are monodentate while the remaining ligand is generally a leaving group, often a halogen. An inherent advantage of these compounds is that the arene rings are hydrophobic, that makes it easy for the Ru(II) complexes to go across the hydrophobic layer of phospholipids in the cell membrane and enter into the cells.[17] The mechanism proceeds via the halogen group undergoing aquation which is reported to be the rate determining step, often succeeded by binding to the phosphate group of a DNA nucleotide.[18,19] Introduction of an aryl group has been observed to significantly amplify this water exchange rate causing an enhancement in the reactivity of the complexes by lowering its pk_a value.[20,21]

RAPTA compounds are a special type of arene ruthenium(II) complexes having a monodentate phosphine ligand PTA (1,3,5-triaza-7-phosphaadamantane). The ligand PTA is chosen because of its good solubility in water and its property to get protonated first in an acidic environment.[22] RAPTA-C (containing two chloride ligands and a p-cymene as the arene moiety) and RAPTA-T (containing two chloride ligands and toluene as the arene moiety) were found to be not very cytotoxic, but they successfully stopped metastasis in the lungs of mice that were infected with mammary carcinoma. It is also reported that RAPTA-C is effective against colorectal and ovarian cancers.[17]

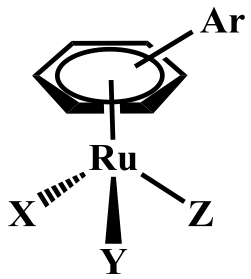

***Figure 1.3**: General structure of Ru arene complex with the formula [(η^6-arene)Ru(X)(Y)(Z)].*

Among other explored Ru metallodrugs, imidazolium trans-[tetrachloro (dimethylsulfoxide)(imidazole)ruthenium (III)] and indazolium trans-[tetrachlorobis(1H-indazole)ruthenium (III)] which is abbreviated as NAMI-A and KP1019 respectively (Figure 1.4), entered into the clinical trials, but the studies were put to rest due to transient nephrotoxicity caused by NAMI-A and poor solubility in water of KP1019.[23–26] However, two other complexes, [Ru(η^6-p-cymene)Cl_2(1,3,5-triaza-7-phosphaadamantane)] or RAPTA-C, and KP1339 which is the sodium salt of KP1019 are currently undergoing clinical trials.

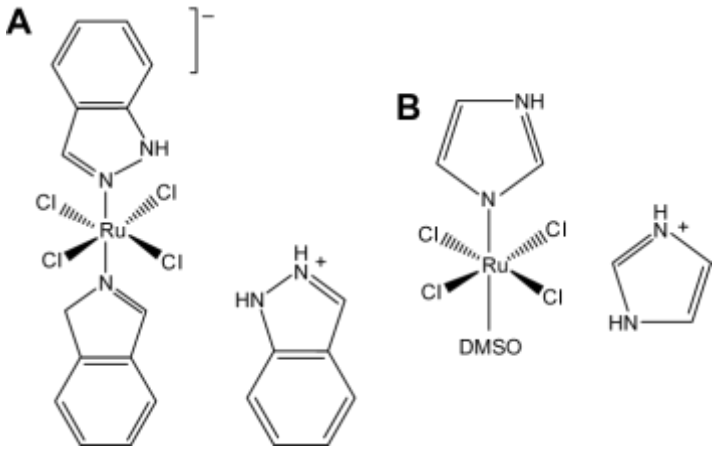

***Figure 1.4**: Structure of (A) KP1019 and (B) NAMI-A.*

1.5 Importance of Ligands

Importantly, the selection of the arene ring, the ligand which chelates to the metal centre and the leaving group has a marked significance on the activity of the drugs.[28] A recent study found that increasing alkyl chain length or aromatic conjugation at the C- or N-terminals of Ru(II)-p-cymene complexes using acylthiourea ligands increased both lipophilicity and anticancer activity.[29] In another study by Prabaharan et al., among the six Ru (II) arene complexes incorporated with the ligand, 2-furyl methyl benzhydrazone, the complex with electron donating methoxy group as the ligand substituent exhibited the highest cytotoxicity because of its electron donating nature.[23] Ru(II) complexes with salicylate ligand has been shown to selectively target the activity of thioredoxin reductase which is often found in excess in tumor cells and thus promote the generation of reactive oxygen species (ROS), which ultimately results in apoptosis of A549 cancer cells.[30] Further, there are reports of utilization pyrene and thiophene containing Schiff bases, tetrazole and picolinamide derivatives, and certain NSAIDs or non-steroidal anti-inflammatory drugs were utilized as ligands to obtain metallodrugs with excellent antiproliferative activities via various mechanism of actions in the recent past.[31–36]

1.6 Organization of the Thesis

Chapter 1: This chapter briefly describes about cancer, the importance of metals in medicine and cisplatin, the emergence of ruthenium compounds as an alternative chemotherapeutic path, the efficiency of ruthenium arene compounds in particular and the importance of choice of ligands.

Chapter 2: This chapter contains the motivation behind this work and review of some of the past work done in this topic.

Chapter 3: This chapter includes the materials, instrumentation, procedure for the synthesis of ligands and complexes and experimental techniques for studying DNA and protein interactions, cytotoxicity assay, lipophilicity study and Hoechst staining process.

Chapter 4: This chapter discusses the results obtained.

Chapter 5: This chapter summarizes the work reported in this thesis and discusses about the future scope of the project.

CHAPTER 2 Past Work

2.1 Review of Past Work and Project Motivation

In one of the recent reports by Pragti et al., cytotoxicity of four Ru(II) arene complexes with 2-aminomethyl pyridine and Cl/PPh_3 as coligands and SO_3CF_3/PF_6 as counter anions are studied (Figure 2.1). It was found that the fluorescence spectrum of HSA got quenched on gradual addition of the complexes, indicating good binding between the complexes and proteins. Among the four, complex **3** showed maximum interaction with the proteins since it consists of a lipophilic isopropyl and a methyl group on the p-cymene and a PPh_3 group as coligand causing an enhanced lipophilicity.

UV–Vis spectroscopy was utilized to study how the complex interacted with DNA. With the increase in CT-DNA concentration to the complexes, hyperchromism was observed suggesting that the DNA and complex are not binding via intercalation but instead via groove binding. Competitive fluorometric titration was performed whereby with increasing amount of complex **1-4** to DNA – DAPI solution, the fluorescence intensity of DNA-DAPI complex decreases as DAPI is displaced by complexes. This further confirms that the complexes utilize groove binding to bind to the complexes. Complexes **3** and **4** showed the maximum binding because of the presence of hydrophobic PPh_3 groups.

MTT Assay showed that complex **3** has the highest cytotoxicity due to PPh_3 group and p-cymene groups causing greater lipophilic interaction with targeted biomolecules. The complexes also have the ability to oxidize NADH to NAD^+ thus over-producing Reactive Oxygen Species (ROS) thereby killing cancerous cells. This hydride transfer from NADH to Ru(II) occurs via ring slippage mechanism.[32]

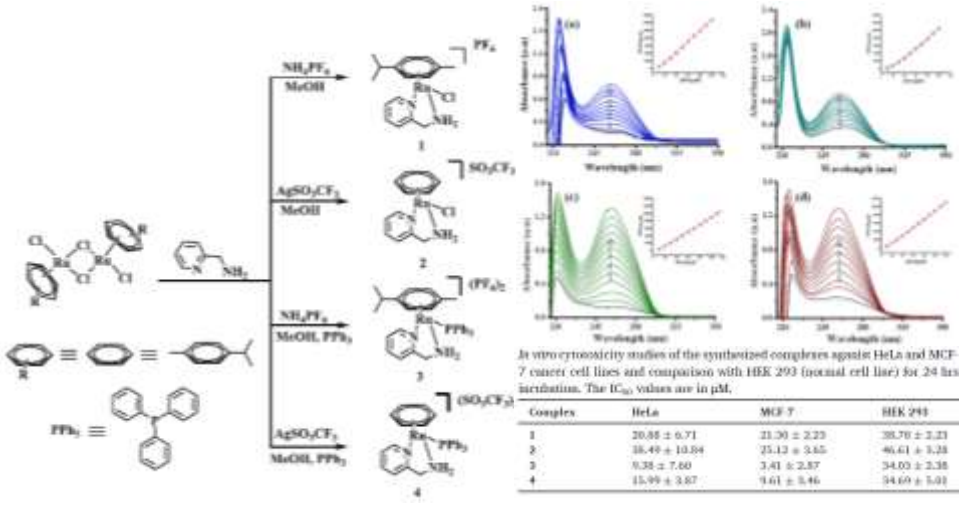

In vitro cytotoxicity studies of the synthesized complexes against HeLa and MCF-7 cancer cell lines and comparison with HEK 293 (normal cell line) for 24 hrs incubation. The IC_{50} values are in μM.

Complex	HeLa	MCF-7	HEK 293
1	20.88 ± 0.71	21.30 ± 2.23	38.78 ± 2.23
2	38.49 ± 10.84	25.12 ± 3.65	46.61 ± 3.28
3	9.38 ± 7.60	3.41 ± 2.87	34.03 ± 2.38
4	15.99 ± 3.87	9.61 ± 3.46	34.69 ± 3.01

Figure 2.1*: Reaction scheme, DNA binding curve, IC_{50} values of the complexes synthesized in reference number 32.*

In another paper, ruthenium(II) arene complexes with naphthalimide moieties which are known to be DNA intercalators are reported as anticancer agents[37]. In one of the series, the naphthalimide unit is attached to the arene and in the other via an imidazole ligand (Figure 2.2).

All the synthesized complexes are found to be more cytotoxic than RAPTA complexes, more selective towards cancerous cells and also effective against those cancer cells which have become cisplatin resistant. Moreover, the compounds which have a substitution of NMe_2 with the naphthalimide group are more active than the ones without substitution since internal charge transfer enhances intercalation and thus toxicity.

The target inside the cell for these compounds is not only the DNA but also the protein as ruthenium is found to preferentially bind to proteins while the naphthalimide part interacts with the DNA. This two way mechanism is a possible reason for the increased cytotoxicity when compared to RAPTA-C.[37]

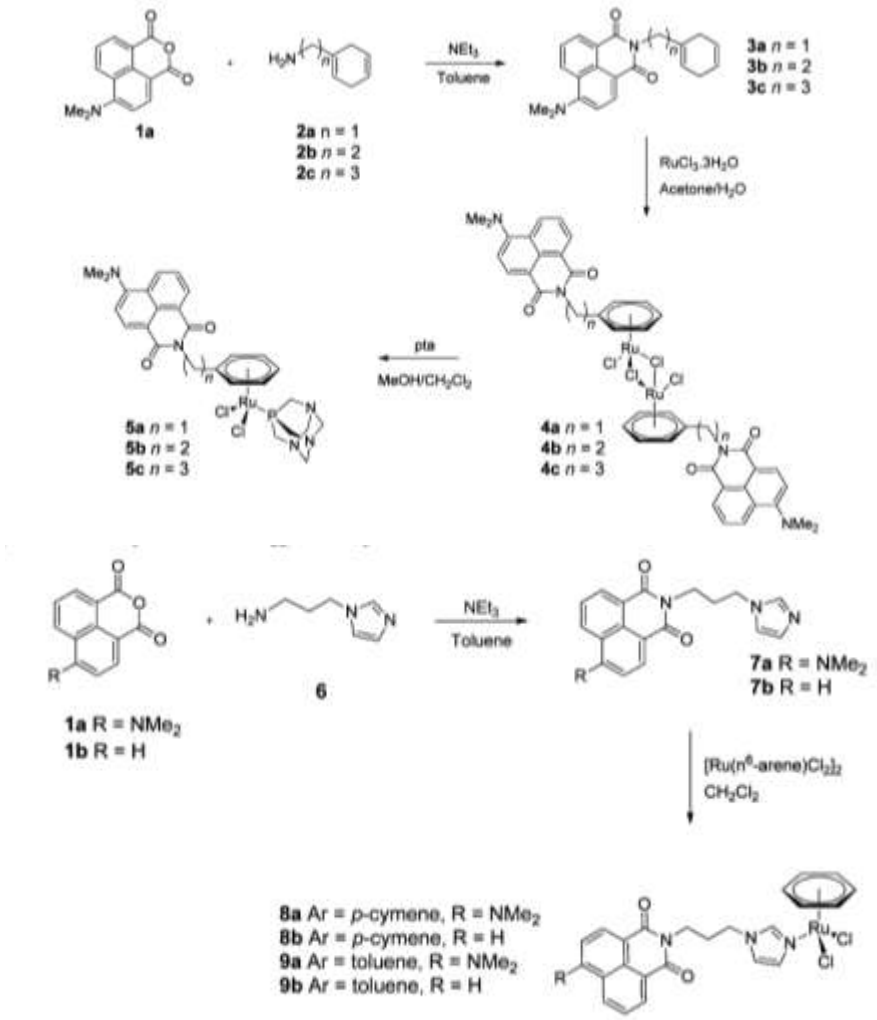

Figure 2.2*: Synthesis of naphthalimide tagged Ru complexes synthesized in reference number 37.*

Two other piano-stool complexes [(η^6-p-cym)M(L)Cl]Cl (where and L= thiosemicarbazone ligand and M= Ru, Os) were synthesized and reported by Gatti et al. (Figure 2.3). From ^{1}H NMR it could be seen that interconversion between E and Z isomers took place in a protic solvent like methanol. The mechanism proceeds through the abstraction of the acidic aromatic ring proton by the solvent. The interconversion between the isomers is proved by NOSEY where the ligand's iminic hydrogen interacts with the protons which are aromatic which is possible only in the Z isomer.

The complexes are cytotoxic enough against HCT116 colon cancer cell lines that they are 20 times more potent compared to the ligand alone. Also, all the complexes collectively have lower resistance factors than cisplatin. Especially ruthenium complex **3** is seen to overcome cisplatin resistance as seen for A2780 ovarian cancer cell lines.[38]

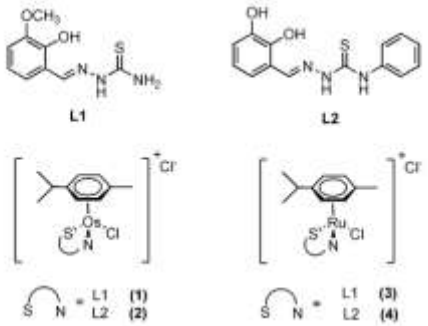

compound	cell lines IC_{50} (μM)				
	A2780	A2780Cis	A549	HCT116	PC3
L1	0.85 ± 0.03	0.12 ± 0.02	42 ± 2	30.6 ± 0.5	6.1 ± 0.1
L2	0.27 ± 0.02	1.23 ± 0.08	23 ± 1	33 ± 5	4.6 ± 0.2
1	1.60 ± 0.02	6.6 ± 0.9	2.4 ± 0.2	24 ± 2	21 ± 1
2	0.75 ± 0.08	7.2 ± 0.1	17 ± 1	2.7 ± 0.2	1.60 ± 0.08
3	4.2 ± 0.3	5.6 ± 0.8		10.5 ± 0.3	19 ± 1
4	0.36 ± 0.03	1.25 ± 0.06		1.64 ± 0.08	1.38 ± 0.04
CDDP	1.2 ± 0.2	13.5 ± 0.3	3.1 ± 0.2	5.2 ± 0.1	9.8 ± 0.4

[a]Clinical drug cisplatin (CDDP) is used as positive control.

Figure 2.3*: Reaction scheme and IC_{50} values of complexes synthesized in reference number 38.*

In the past, the anti-inflammatory, antitumor, antibacterial, antiviral, antiparasitic and antifungal properties of biologically active benzimidazole based ligands have been studied extensively since a similar kind of core structure exists in various pharmaceutical compounds (Figure 2.4).[39–42] Ru(II) complexes using benzimidazole based ligands like 2-aminophenyl benzimidazole[43] and methyl 1-butyl-2-arylbenzimidazolecarboxylate[44] have been synthesized in the recent past that showed strong binding capabilities with CT-DNA and consequently showed strong cytotoxicity against cancer cells. Apart from attacking the DNA in the nucleus, cell death might also be caused due to production of superoxide anions caused by mitochondrial damage as shown in a work with Ru(II) complex with a bis-benzimidazole derivative ligand.[45] In another study[46], a series of Ru(II)

arene complexes using 2-pyridin-benzimidazole and 2-phenyl-benzimidazole based ligands was synthesized with the arene part varying between p-cymene, benzene and phenoxyethanol. The cytotoxicity was found to be associated with a dual mode of binding to CT-DNA via covalent interaction and intercalation, with the p-cymene complexes showing a higher activity.

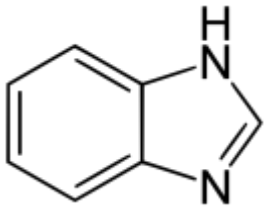

Figure 2.4*: Structure of benzimidazole moiety.*

Inspired by these findings, three Ru(II)-arene complexes have been synthesized in this work where a fluorescent benzimidazole derivative ligand has been incorporated while varying the coligand coordinated in the sixth position.

CHAPTER 3 Experimental Section

3.1 Reagents and Chemicals

All of the chemicals bought from Sigma Aldrich, India and Alfa Aesar were highly purified and were no more purification has been done before use. Chemicals like PBS buffer and MTT (3-(4,5-dimethylthiazol-2-yl)-2,5-diphenyltetrazolium bromide) were purchased from Himedia Chemical, India. The experiments were carried out in open atmosphere.

3.2 Methods and Instrumentation

For recording ESI-MS spectra, mass spectrometer from Bruker-Daltonics, microTOF-Q II was utilized. Bruker AVANCE III 400 MHz Ascend BioSpin was used to record the proton ^{1}H and ^{13}C NMR data. Tetramethylsilane was used as reference for recording NMR. Fourier Transfer Infrared data was obtained using KBr pellets by a Tensor 27 FTIR spectrometer from Bruker whose range was from 4000 to 500 cm^{-1}. Fluorometric experiments were conducted in HORIBA's Fluoromax-4 (model no. FM-100) spectrofluorometer with a quartz cuvette of path length 1 cm at 25.0 ± 0.2 ºC. Spectrophotometric measurements for absorption study were done by using a similar cuvette on a Varian UV-Vis spectrophotometer (Model: Cary 100). A Perkin-Elmer lambda-650 DRS UV-Visible spectrophotometer, equipped with an integration sphere diffuse reflectance attachment (range 200-1200 nm) against $BaSO_4$ as reference was utilized for UV-Vis analyses. Staining assay was done with the help of confocal microscope Fluoview FV100 (OLYMPUS, 449 Tokyo, Japan).

3.3 Synthesis of Ligand and Metal Complexes

3.3.1 Synthesis of Ligand 2-(1H-benzo[d]imidazol-2-yl)-6-methoxyphenol (HL)

Synthesis of ligand was performed using a previously reported method.[47] To synthesize the ligand, ortho-vanillin (0.152 g, 1 mmol), 1,2-phenylene diamine (0.108 g, 1 mmol) and sodium bisulphite (0.150 g, excess) was made to dissolve in N, N-dimethylformamide (DMF) and the reaction was carried out for 12 hours in reflux conditions. The solution was then made to cool down and ice cold water was used to quench the reaction. The resulting precipitate was filtered and thoroughly washed with MQ-H_2O and dried to obtain a creamy white product. Yield: 0.179 g, 75%.

3.3.2 Synthesis of [Ru(η^6-p-cym)(L)Cl] (1)

To obtain complex **1**, the synthesized ligand **HL** (0.039 g, 0.16 mmol) in MeOH (10 mL) was added in a dropwise manner to a 10 mL methanol solution of the Ru(II) dimer [(η^6-p-cymene)$RuCl_2$]$_2$ (0.050 g, 0.08 mmol) which was then made to stir at 25^{o}C for 6 hours. The solvent was then made to evaporate using high vacuum to obtain an orange-brown compound. Yield: 0.082 g, 68%.

3.3.3 Synthesis of [Ru(η^6-p-cym)(L)PPh_3]PF_6 (2)

To synthesize complex **2**, triphenylphosphine (PPh_3) (0.042 g, 0.16 mmol) was made to dissolve in 10 mL methanol and mixed with a solution containing complex **1** (0.082 g, 0.16 mmol) and 15 mL MeOH. The reagents were then stirred for 12 hours at the normal room temperature. After the reaction is completed, to the intermediate solution, a solution of ammonium hexafluorophosphate (NH_4PF_6) (0.026 g, 0.16 mmol) and methanol was added and further kept for stirring at room temperature for 2 hours further. After the reaction was carried out, the solvent from the mixture was made to evaporate under high vacuum and an orange-brown

product was obtained. Yield: 0.077 g, 65%.

3.3.4 Synthesis of [Ru(η^6-p-cym)(L)(PTA)]PF_6 (3)

Synthesis of complex **3** was carried out by adding 1,3,5-triaza-7-phosphaadamantane (PTA) (0.025 g, 0.16 mmol) in methanol to a mixture of complex **1** (0.082 g, 0.16 mmol) and MeOH in a dropwise manner after which the reagents were kept for stirring for 12 hours at room temperature. After that ammonium hexafluorophosphate (NH_4PF_6) (0.026 g, 0.16 mmol) dissolved in methanol (10 mL) was added into the solution and further stirred for another 2 hours at 25^{o}C. Then using a vacuum, the solvent was made to evaporate to obtain a reddish brown compound. Yield: 0.076 g, 65%.

3.4 Lipophilicity Study

The lipophilicity of complexes quantified by log P values was determined using the shake-flask procedure with two phases, one of which was a mixture of pure water (HPLC grade) and DMSO and the other being an n-octanol phase. Initially, the optical densities of the complexes were measured separately at three different concentrations in both octanol and a mixture of water and DMSO (2:1) (due to poor solubility in water). From the slope of absorbance vs. concentration plot, the extinction coefficient was calculated. 5 mg of the compounds were taken in a solution comprising of 10 mL water-DMSO and 10 mL octanol. The two phases were then shaken for duration of 15 minutes and kept isolated to equilibrate for 24 hours at 25^{o}C. After the two phases separate, 1 mL of the complex in both the phases was separated and the concentration was determined spectrophotometrically, by the Lambert Beer's law from the absorbance of the spectra obtained.[48] $P_{o/w}$ value was calculated according to the equation:

$$P_{\mathrm{o/w}} = \frac{concentration\ in\ octanol}{concentration\ in\ water} \quad \ldots(1)$$

3.5 Protein Binding Study

Tryptophan fluorescence quenching assays with human and bovine serum albumin (HSA and BSA respectively) were used to determine the amount of protein binding by the produced compounds. The HSA and BSA excitation wavelengths were 280 nm and the quenching of the emission intensity at 345 nm was measured with increasing concentrations of the quencher (ligand **HL** and complexes **1**-**3**). Throughout the experiment, the widths of the excitation and emission slits, as well as the scan speeds, were kept constant. With Tris buffer solution (strength = 50 mM), a stock solution of BSA/HSA (strength = 10 μM) was prepared and kept at 4 °C for future use. Synthetic chemicals were used to make stock solutions with a concentration of 5 mM. The fluorescence intensity was measured as a blank in a fluorometric titration using 2 mL of protein solution. For titration in each step, 2 μL stock solution was added to the solution of BSA/HSA, and the fluorescence intensity was evaluated. To quantify fluorescence quenching, upto a total volume of 20 μL compound's stock solution was added to the working cuvettes. The quenching of fluorescence was further examined using the Stern–Volmer equation[49], which is as follows:

$$\frac{F_0}{F} = 1 + K_q \tau_0 [Q] = 1 + K_{SV} [Q] \quad \ldots (2)$$

where F_0 and F are the fluorescence intensities when a quencher is excluded and included respectively in the experiment, K_q stands for the bimolecular quenching rate constant, τ_0 is the fluorophore's average lifespan without a quencher, and [Q] is the quencher concentration (metal complexes). K_{SV} in M^{-1} stands for the Stern–Volmer quenching constant. The following formula is used to compute the binding constant K_a and the number of complexes bound to the protein (n). [32]

$$\log\left[\frac{(F_0 - F)}{F}\right] = \log K_a + n \log[Q] \quad \ldots (3)$$

3.6 DNA Binding Study

3.6.1 Absorption spectroscopy

Metal complexes' interactions with DNA were investigated using the electronic absorption approach. Calf thymus, also known as CT-DNA was kept at 4^{o}C. CT-DNA in a solution of NaCl (50 mM) and Tris in water (5 mM, pH = 7.2) provided an absorbance ratio of 1.9 (A_{260}/A_{280}, A = absorbance at 260 and 280 nm) in the UV spectra, showing that protein was absent in the DNA. After 1:100 dilutions, the DNA concentration was determined by measuring the extinction coefficient or the ϵ value at 260 nm. Stock solutions of the complexes were generated by weighing the required amount of complexes and dissolving the same in DMSO. They were kept at 4^{o}C and utilized within four days. Titrations of absorption spectra were performed at 25^{o}C in the buffer solution that was prepared to study the ability of the complexes to bind to the CT-DNA. The concentration of the complex was kept constant at 10 μM while it was titrated against the DNA solution whose concentration was increased gradually (0-150 μL).[49]

3.6.2 Emission spectroscopy

The complex's binding ability to CT-DNA was measured with via fluorometric titration of a DAPI- DNA solution in Tris-HCl (5 mM)/NaCl (50 mM) buffer (pH=7.4). For 30 minutes, CT-DNA was incubated with DAPI at a ratio that was predetermined ([DNA]/[DAPI] = 2.0). The quenching impact on fluorescence after complex addition to this solution was studied by recording the fluorescence data (excitation wavelength = 350 nm, emission wavelength = 458 nm). The experiment was conducted by maintaining a constant strength of the solution of DNA and DAPI in buffer ([CT-DNA] = 10 μM and [dye] = 15 μM). To this, the stock solutions of the complexes were added with an increment of 10 μL in each step until 150 μL volume. after which the fluorescence was recorded.[49]

3.7 Cytotoxicity Assay

Cell lines were acquired from NCCS or National Centre for Cell Sciences. It was grown in Dulbecco's Modified Eagles medium (DMEM) containing fetal bovine serum (FBS, 10%), penicillin (100 g/mL), L-glutamine (200 mM), and streptomycin (10 mg/mL) at 37^{o}C in a humid environment with CO_2 (5%). Cells were cultivated and grown in a logarithmic growth phase until the cell count reached 1.0×10^6 cells/mL.

3.7.1 Evaluation of cytotoxicity

The complex's cytotoxicity against MCF-7 and HeLa cells was determined using the MTT [3-(4, 5-dimethylthiazol-2-yl)-2, 5-diphenyltetrazoliumbromide] test. To summarize, all cells were seeded (5×10^4 cells/well) on a 96-well plate and maintained for 24 hours in a CO_2 environment to grow. Cells were then incubated for 24 hours with varying doses (0.25-100 μM) of compounds (in a solution of DMSO or H_2O). The culture media was withdrawn after incubation, and 10 μL of the PBS solution of MTT (conc. = 5 mg/mL) was added to each well. MTT was removed following incubation in the dark for 4 hours, and DMSO or H_2O (100 μL to each well) was added to make the formazan formed (purple) soluble. The experiment was repeated three times. Colorimetric analysis was conducted with an ELISA microplate reader at 570 nm. The cell viability percentage was computed and represented as follows: percent cell viability = (OD value of cells that were treated)/ (OD value cells that were untreated (control)) × 100.[49,50] Using the Prism GraphPad software tool IC_{50} values or the concentration of the dose of a complex that destroyed 50% of the cells was calculated using the plot of OD vs concentration. The IC_{50} values given are mean ± SEM.

3.8 Hoechst Staining

Hoechst stain 33258 was used to examine the morphology of the cells. The 5×10^4 HeLa cells were put in six-well plates with a coverslip in each well and cultured in a CO_2 incubator overnight for adhesion. The cells were subsequently treated with the complexes at their IC_{50} concentrations and kept for one whole day while untreated cells served as controls. These cells were then fixed with 4% paraformaldehyde and were made permeable with 0.1 percent Triton × 100. These cells were then stained at 25^oC for 30 minutes with the dye Hoechst 33258 (5 μg/mL) before being washed with PBS buffer. The coverslips were then put on glass slides and the fluorescence was examined using an OLYMPUS confocal microscope.[51,52]

CHAPTER 4 Results and Discussion

4.1 Structure and Synthesis

Three Ru(II) arene complexes (**1-3**) with pseudo-octahedral geometry where three coordination sites are occupied by a p-cymene ring have been synthesized and characterized. Two of the other coordination sites are taken up by the synthesized benzimidazole derivative ligand (**HL**) whose O and N act as donor centres. The sixth position of the pseudo-octahedral complex is involved in coordination with a ligand that varies between Cl, PPh_3 or PTA. PPh_3 was used as coligand because it is expected to increase the lipophilicity while PTA is expected to increase the solubility in water. The objective of this work is also to test the effect of solubility on the cytotoxicity of the synthesized complexes. Compound **2** and **3**, which are cationic in nature are treated with ammonium hexafluorophosphate salt to counter balance the charge of the compound. The chlorido complex **1** was synthesized by reacting the Ru dimeric precursor with the previously synthesized ligand (**HL**) which was further treated with PPh_3 or PTA followed by the necessary counteranions in excess as required for obtaining complexes **2** and **3** (Scheme 4.1, Scheme 4.2).

4.2 Reaction Schemes

4.2.1 Synthesis of Ligand (HL)

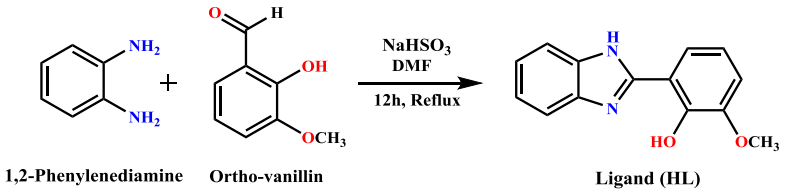

Scheme 4.1: *Reaction scheme for the synthesis of ligand (**HL**).*

4.2.2 Synthesis of Complexes 1-3

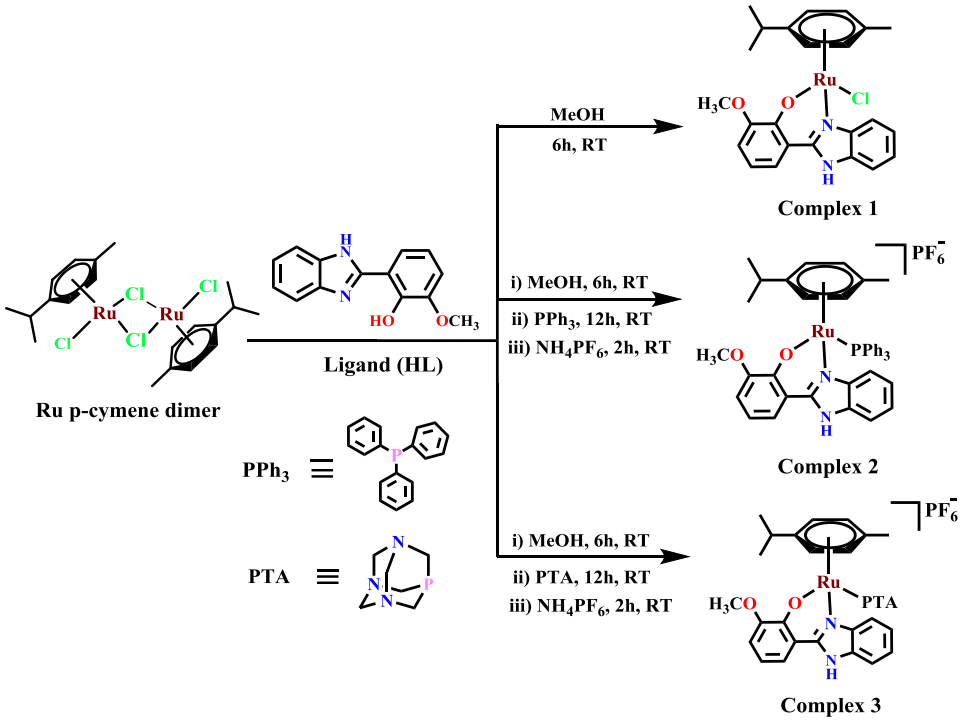

Scheme 4.2: *Reaction scheme for the syntheses of complexes **1-3**.*

4.3 Characterization

4.3.1 Mass Spectra

All the synthesized compounds were characterized by ESI-MS spectra. The ligand (**HL**) shows a base peak corresponding to $[HL + H]^+$ (Figure 4.1) whereas for complex **1**, the peak is obtained due to the $[RuL(p\text{-}cym)]^+$ fragment (Figure 4.2). Complexes **2** and **3** exhibit peaks in the spectra corresponding to the cationic portion of the complexes themselves in both the cases (Figure 4.3, Figure 4.4).

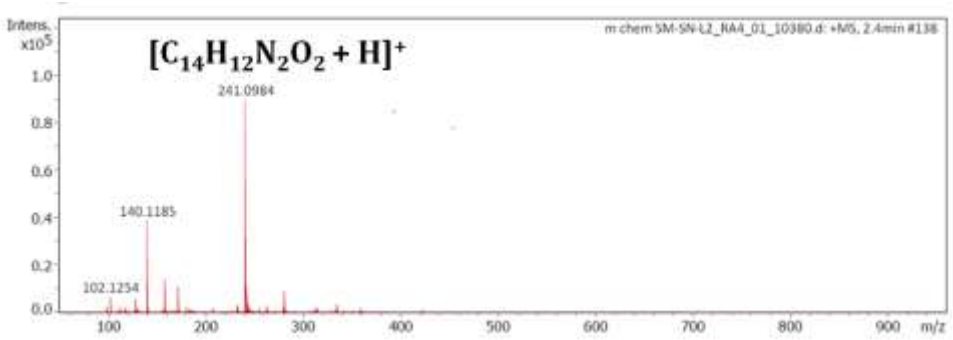

***Figure 4.1**: ESI-MS of ligand (**HL**); ESI-MS (m/z) $C_{14}H_{12}N_2O_2$: Calculated for $[C_{14}H_{12}N_2O_2 + H]^+$: 241.09; Found: 241.0984.*

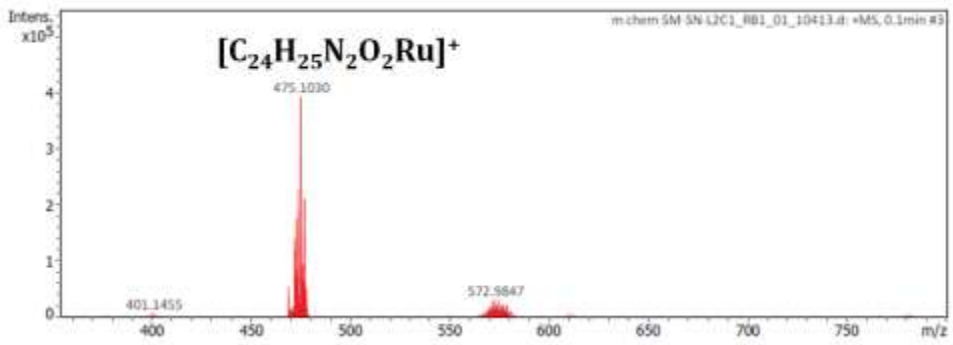

***Figure 4.2:** ESI-MS of complex **1**; ESI-MS (m/z) $C_{24}H_{25}N_2O_2ClRu$: Calculated for $[C_{24}H_{25}N_2O_2Ru]^+$: 475.10; Found: 475.1030.*

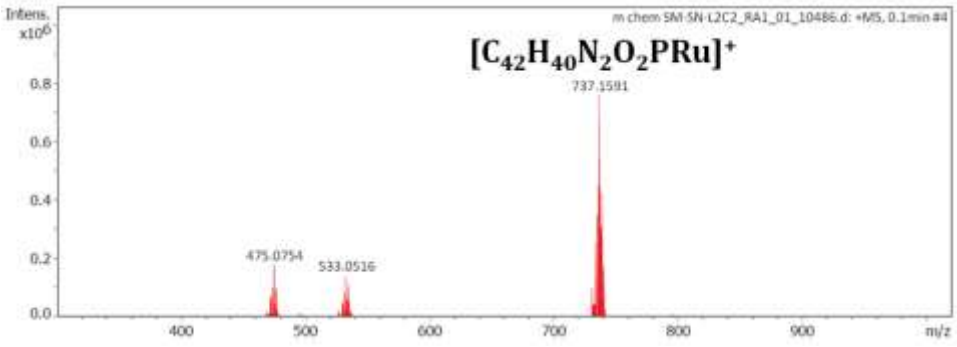

***Figure 4.3**: ESI-MS of complex **2**; ESI-MS (m/z) $C_{42}H_{40}N_2O_2PRu$: Calculated for $[C_{42}H_{40}N_2O_2PRu]^+$: 737.19; Found: 737.1591.*

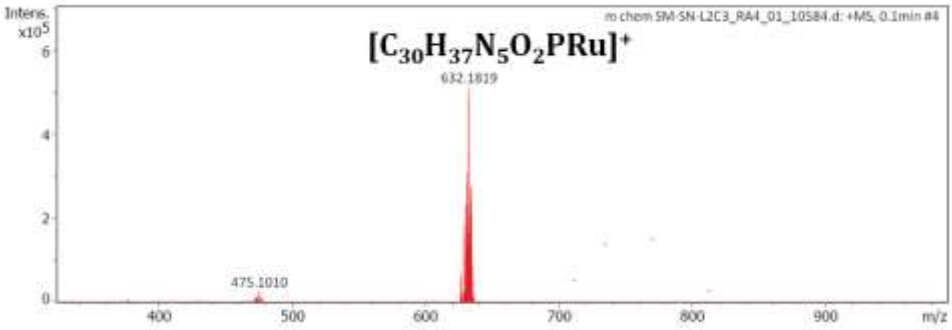

***Figure 4.4**: ESI-MS of complex **3**; ESI-MS (m/z) $C_{30}H_{37}N_5O_2PRu$: Calculated for $[C_{30}H_{37}N_5O_2PRu]^+$: 632.17; Found: 632.1819.*

4.3.2 NMR Spectra

NMR spectroscopic data of complex **1-3** and ligand (**HL**) were found in accordance with the predicted structures. The data was recorded with samples dissolved in DMSO-d_6. The ^{1}H NMR spectra display peaks in the δ 5.71–5.82 ppm region for the p-cymene aromatic protons while the peaks appearing in the δ 6.6 -7.7 ppm region represent the protons of the ligand (**HL**) in the aromatic region. The peaks at δ 2.8, 1.7-2.09, 0.9-1.2 ppm are due to the p-cymene ring side chains and the one around 13.2 ppm arises because of the N-H proton which couples with the OH proton peak in case of the ligand. The PTA protons give peaks in the region δ 4.73-4.26 ppm and the peaks for PPh_3 aromatic ring protons are displayed

in the region δ 7.44-7.15 ppm. The complexes also present a singlet peak due to the methoxy proton at around δ 3.8 ppm.

4.3.2.1 NMR Spectra of Ligand (HL)

^{1}H NMR (400.13 MHz, 298 K, DMSO-d_6) δ, ppm: 13.22, 13.30 [d, H of N-H and O-H], 7.74-6.95 [aromatic protons of the ligand], 3.85 [s, 3H, CH of OCH_3] (Figure 4.5). ^{13}C NMR (100.61 MHz, DMSO-d_6) δ, ppm: 152.40 [C of NH-C=N], 149.05 [C of C-OCH_3], 148.81 [C of C-OH], 123.76, 122.90, 119.17, 118.40, 118.06, 114.38, 112.96, 111.97 [C of ligand], 56.17 [C of OCH_3] (Figure 4.6).

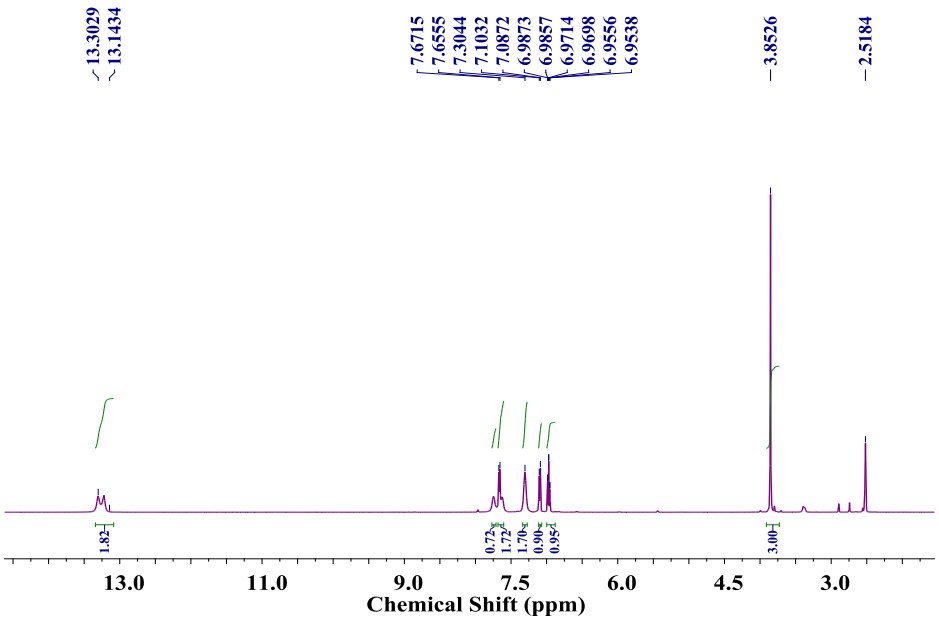

***Figure 4.5**: ^{1}H NMR spectrum of ligand (**HL**).*

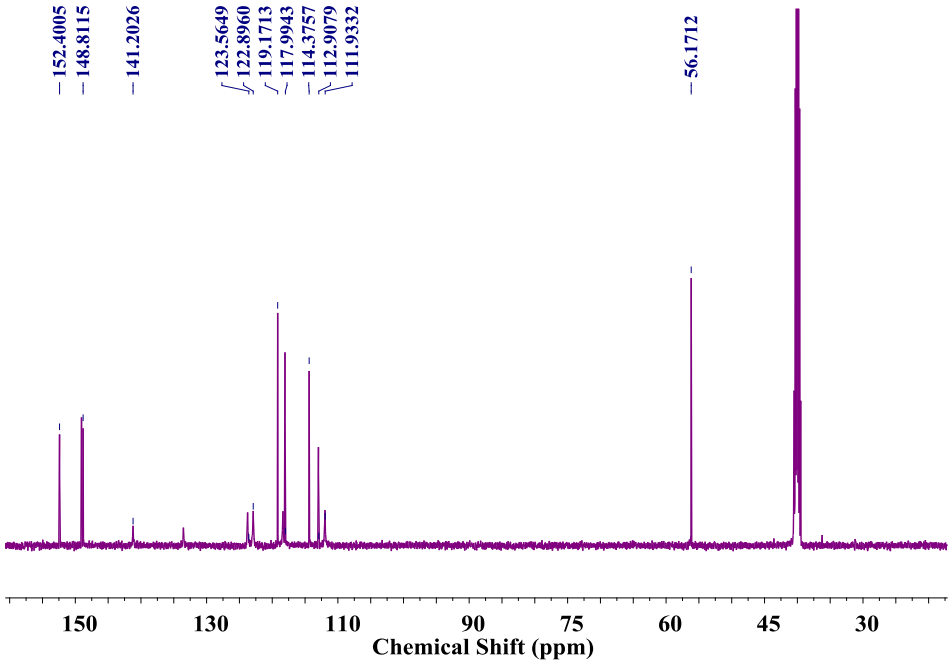

Figure 4.6: *^{13}C NMR spectrum of ligand (**HL**).*

4.3.2.2 NMR Spectra of Complex 1

^{1}H NMR (400.13 MHz, 298 K, DMSO-d_6) δ, ppm: 13.29 [s, 1H, H of N-H], 7.69-6.95 [aromatic protons of the ligand], 5.82-5.77 [aromatic protons of p-cym ring], 3.84 [s, 3H, CH of OCH_3], 2.85 [m, 1H, $CH(CH_3)_2$], 2.09 [s, 3H, CH of $C_6H_4CH_3$], 1.20 [d, 6H, CH of $C(CH_3)_2$] (Figure 4.7). ^{13}C NMR (100.61 MHz, DMSO-d_6) δ, ppm: 152.02 [C of NH-C=N], 149.03 [C of C-OCH_3], 148.68 [C of C-OH], 123.53, 119.28, 118.27, 114.54, 112.75, 106.84, 100.55 [C of ligand], 86.83, 85.97 [C of p-cym ring], 56.24 [C of OCH_3], 30.44 [CH of p-cym ring], 21.96 [CMe_2 of p-cym ring], 18.33 [Me of p-cym ring] (Figure 4.8).

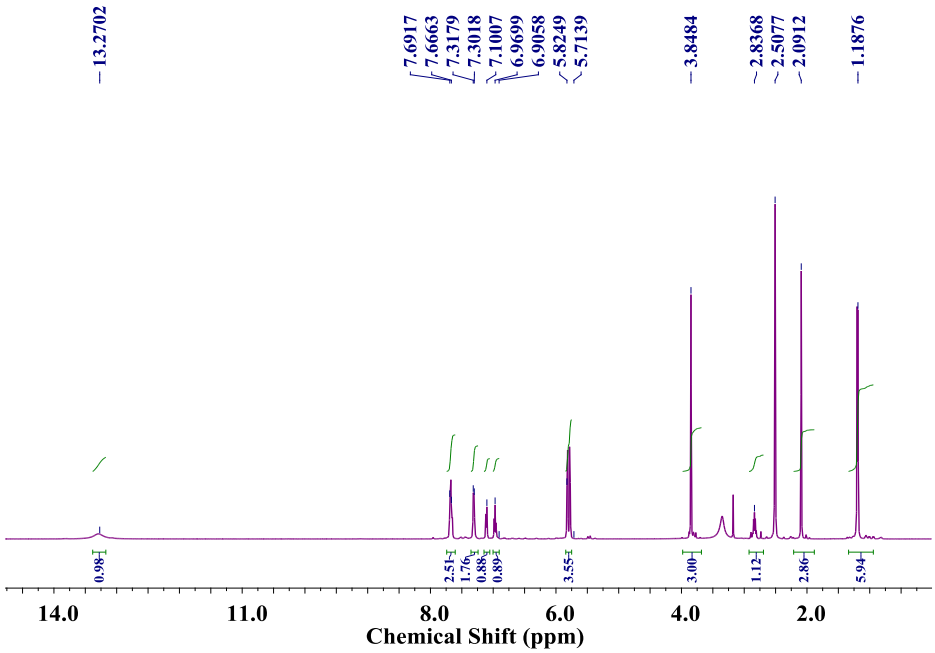

***Figure 4.7**: [1]H NMR spectrum of complex **1**.*

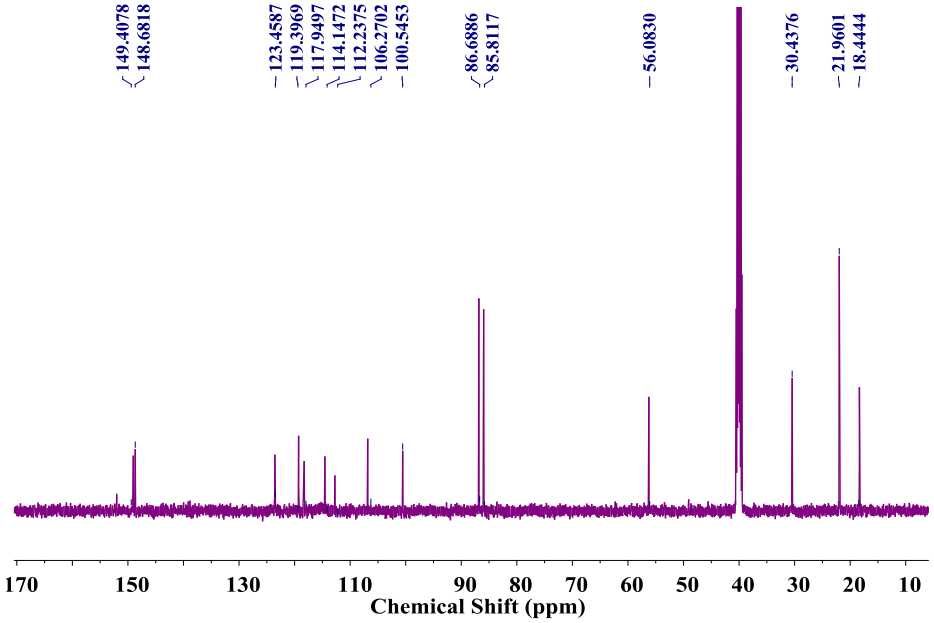

***Figure 4.8**: [13]C NMR spectrum of complex **1**.*

4.3.2.3 NMR Spectra of Complex 2

^{1}H NMR (400.13 MHz, 298 K, DMSO-d_6) δ, ppm: 13.29 [s, 1H, H of N-H], 7.75-6.81 [aromatic protons of the ligand], 7.39–7.22 [aromatic protons of PPh_3], 5.31-5.24 [aromatic protons of p-cym ring], 3.87 [s, 3H, CH of OCH_3], 2.88 [m, 1H, $CH(CH_3)_2$], 1.76 [s, 3H, CH of $C_6H_4CH_3$], 0.92 [d, 6H, CH of $C(CH_3)_2$] (Figure 4.9). ^{13}C NMR (100.61 MHz, DMSO-d_6) δ, ppm: 154.76 [C of NH-C=N], 149.02 [C of C-OCH_3], 148.29 [C of C-OH], 134.55, 130.58, 128.31 [C of PPh_3], 124.31, 123.04, 119.67, 119.07, 118.52, 115.14, 109.00, 102.77 [C of ligand], 90.03, 87.03 [C of p-cym ring], 56.41 [C of OCH_3], 30.18 [CH of p-cym ring], 21.80 [CMe_2 of p-cym ring], 17.55 [Me of p-cym ring] (Figure 4.10). ^{31}P NMR (126 MHz, DMSO-d_6) δ, ppm: -23.91 [s, PPh_3], -144.09 [sept, PF_6] (Figure 4.11).

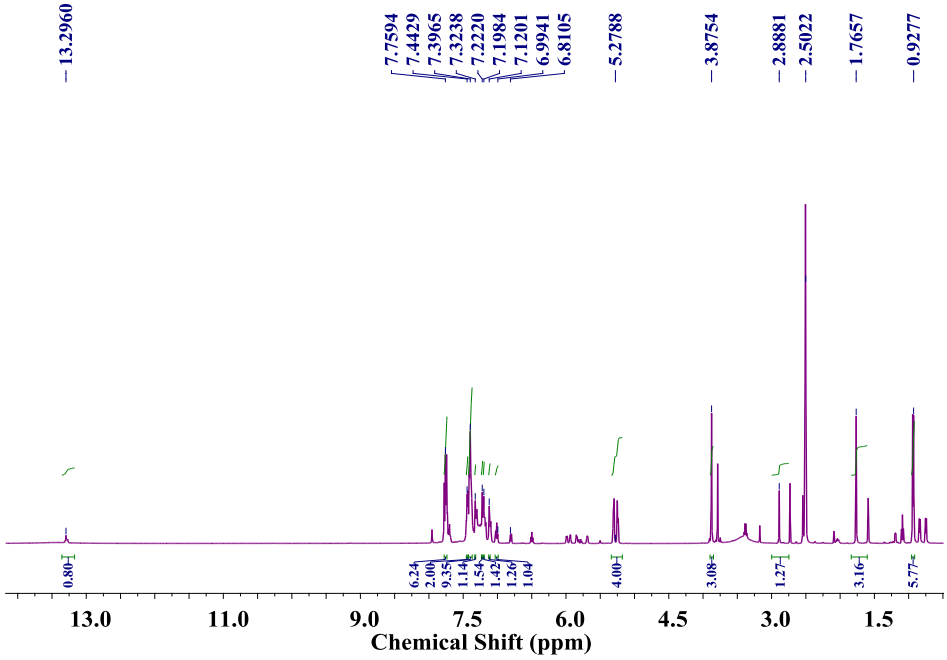

Figure 4.9: *^{1}H NMR spectrum of complex **2**.*

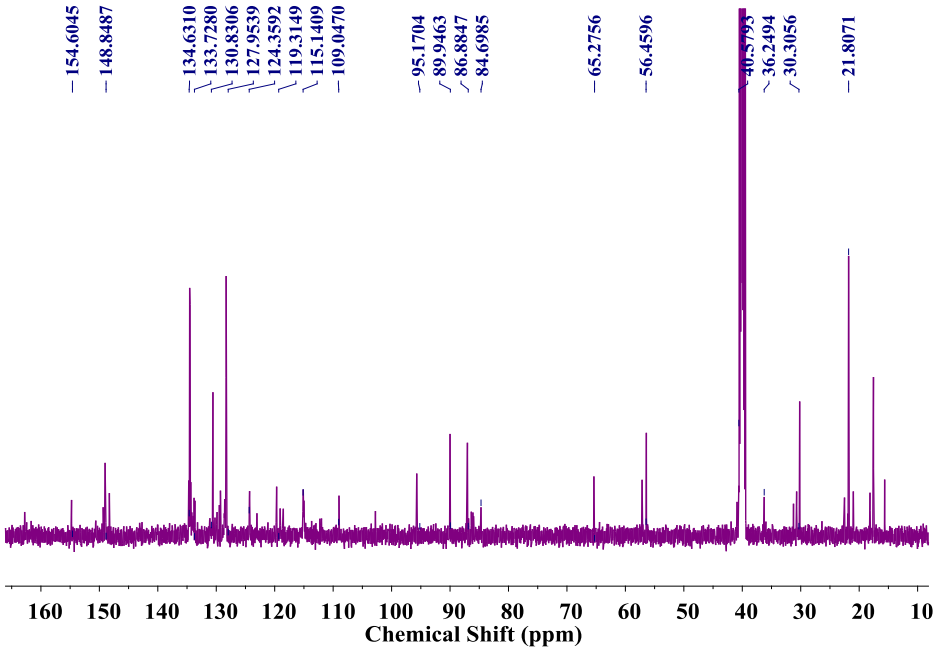

Figure 4.10: *^{13}C NMR spectrum of complex **2**.*

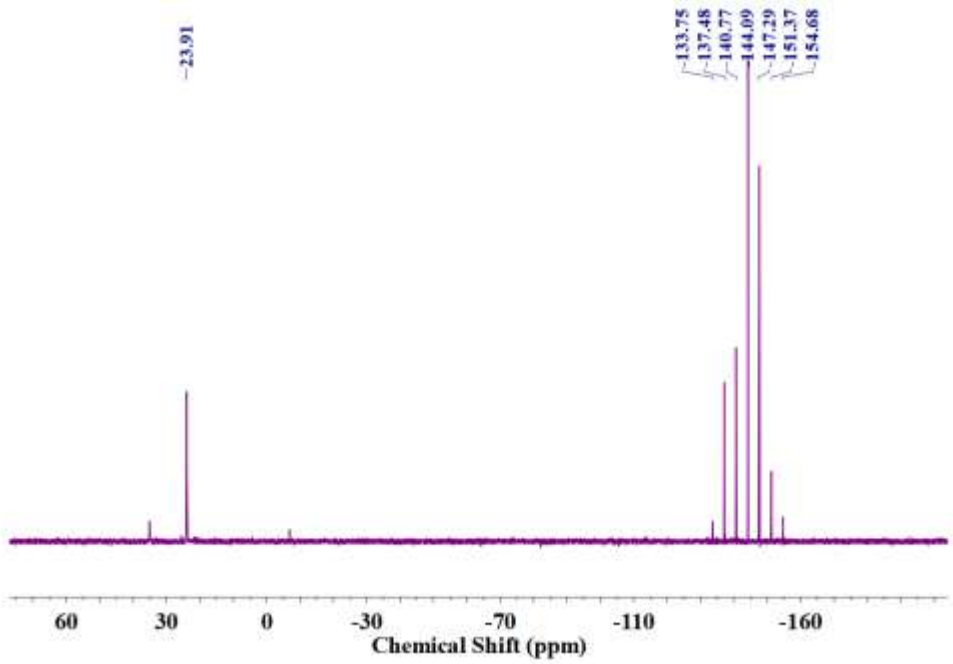

Figure 4.11: *^{31}P NMR spectrum of complex **2**.*

4.3.2.4 NMR Spectra of Complex 3

^{1}H NMR (400.13 MHz, 298 K, DMSO-d_6) δ, ppm: 13.87 [s, 1H, H of N-H], 7.63-6.62 [aromatic protons of the ligand], 5.86-5.84 [aromatic protons of p-cym ring], 4.73 [s, 6H, 3xNCH_2N], 4.26 [s, 6H, 3xPCH_2N], 3.77 [s, 3H, CH of OCH_3], 2.89 [m, 1H, $CH(CH_3)_2$], 1.97 [s, 3H, CH of $C_6H_4CH_3$], 1.12 [d, 6H, CH of $C(CH_3)_2$] (Figure 4.12). ^{13}C NMR (100.61 MHz, DMSO-d_6) δ, ppm: 162.79 [C of NH-C=N], 154.34 [C of C-OCH_3], 142.53 [C of C-OH], 124.57, 123.93, 123.45, 119.24, 118.36, 116.60, 115.41, 114.49 [C of ligand], 89.80, 89.77, 88.86, 88.63, 88.17, 88.13 [C of p-cym ring], 85.74, 85.70 [C of NCH_2N], 71.71, 71.30 [C of NCH_2P] 56.63 [C of OCH_3], 30.60 [CH of p-cym ring], 22.16 [CMe_2 of p-cym ring], 21.68 [Me of p-cym ring] (Figure 4.13). ^{31}P NMR (126 MHz, DMSO-d_6) δ, ppm: −29.53 [s, PTA], −144.19 [sept, PF_6] (Figure 4.14).

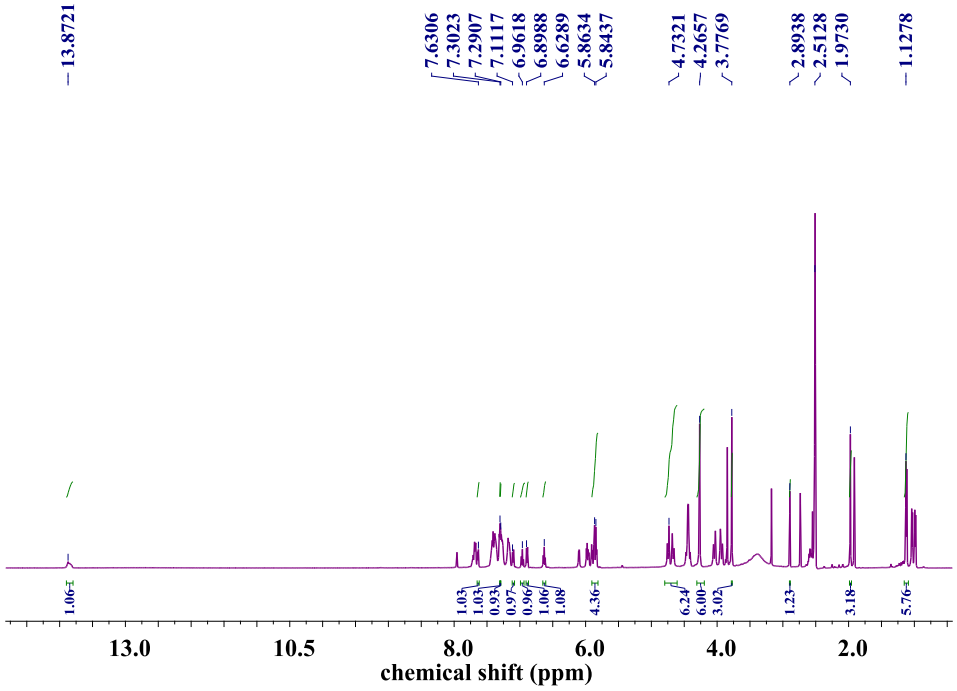

Figure 4.12: *^{1}H NMR spectrum of complex **3**.*

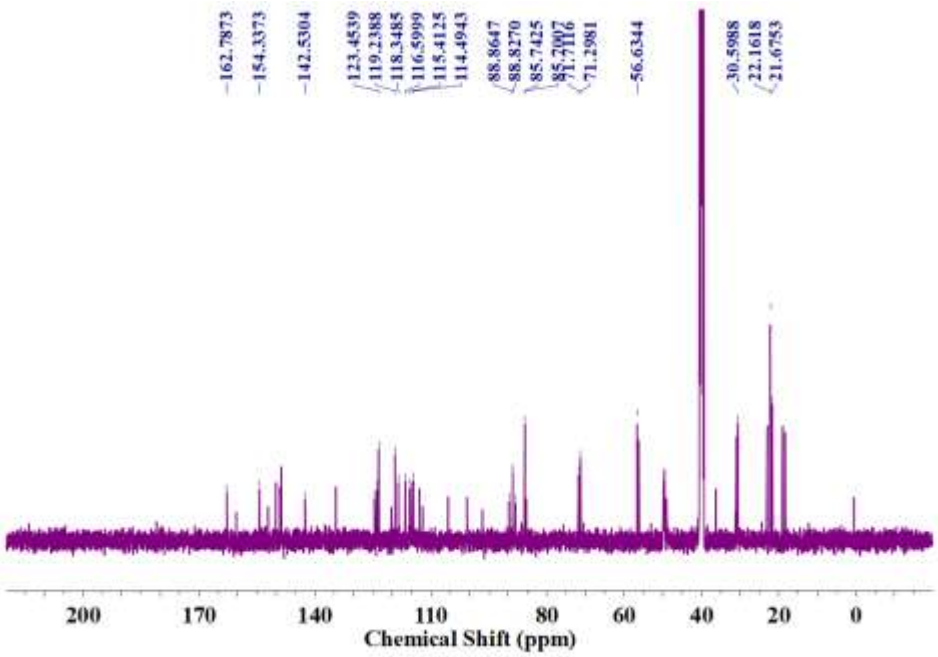

***Figure 4.13**: [13]C NMR spectrum of complex **3**.*

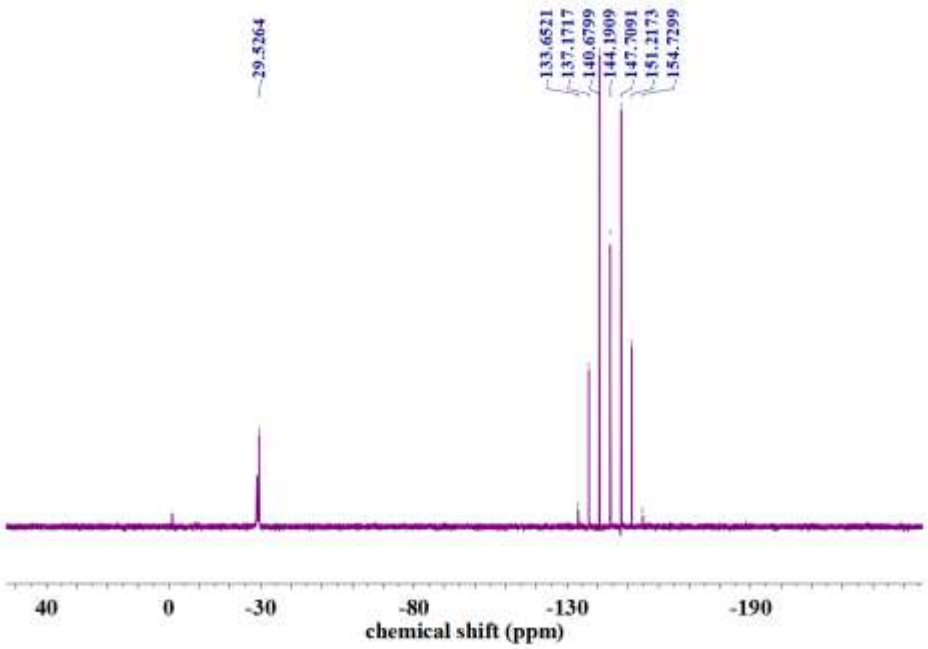

***Figure 4.14**: [31]P NMR spectrum of complex **3**.*

4.3.3 FT-IR Spectra

Fourier Transfer Infrared (FTIR) spectra was measured using the instrument Brunker Tensor 2 FTIR spectrometer using KBr pellets. The peaks of the IR-spectra matched with the expected characteristic bands of various functional groups of the ligands and the complexes.

The FTIR spectra of all the compounds show a peak in the region 1565-1570 cm^{-1} confirming the presence of C=N bond in our compounds.[53] A peak at 1250 cm^{-1} is also observed which corresponds to $\nu_{C\text{-}O\text{-}C}$. The peak for N-H and O-H stretching frequency for all the compounds were found to be overlapping in the range of 3200-3460 cm^{-1}. All the above mentioned peaks are a contribution of the ligand (**HL**) which is present in all the compounds (Figure 4.15). The difference between the spectra of the complexes and ligand is that in that of the complexes peaks for Ru-P or Ru-Cl appeared in the range of 805-846 cm^{-1}. This observation also proves that complexation with Ru was successful (Figure 4.16, Figure 4.17, Figure 4.18).

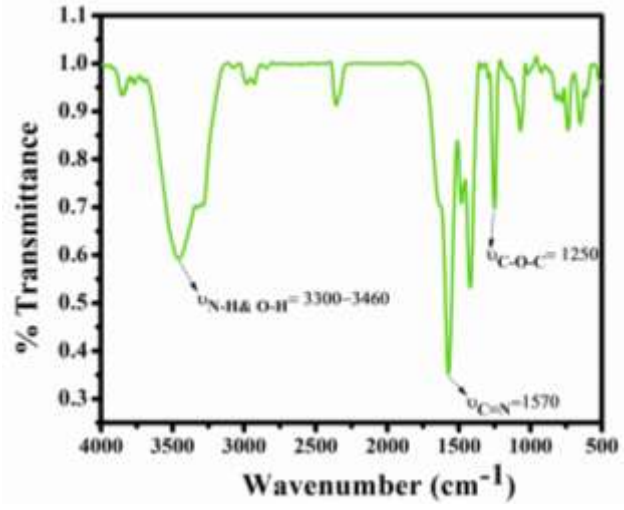

Figure 4.15*: FT-IR spectrum of ligand (**HL**).*

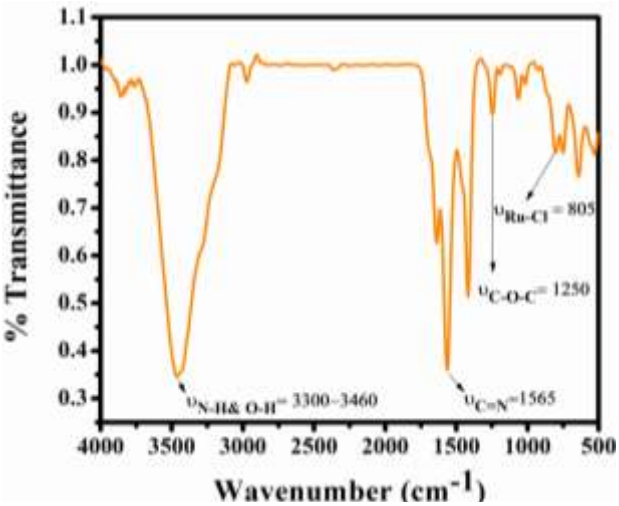

***Figure 4.16**: FT-IR spectrum of complex **1**.*

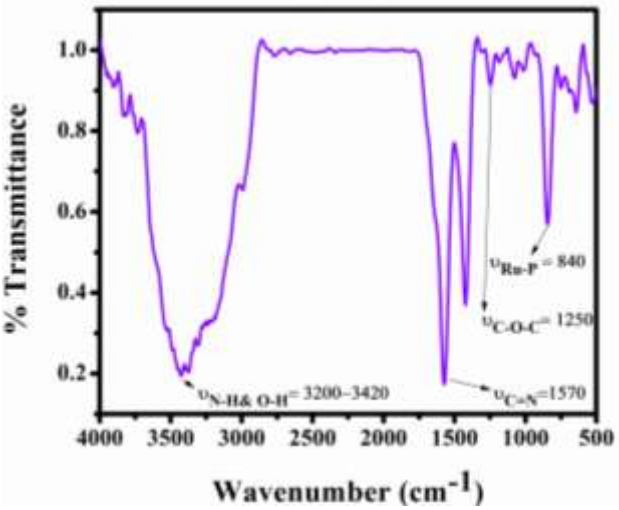

***Figure 4.17**: FT-IR spectrum of complex **2**.*

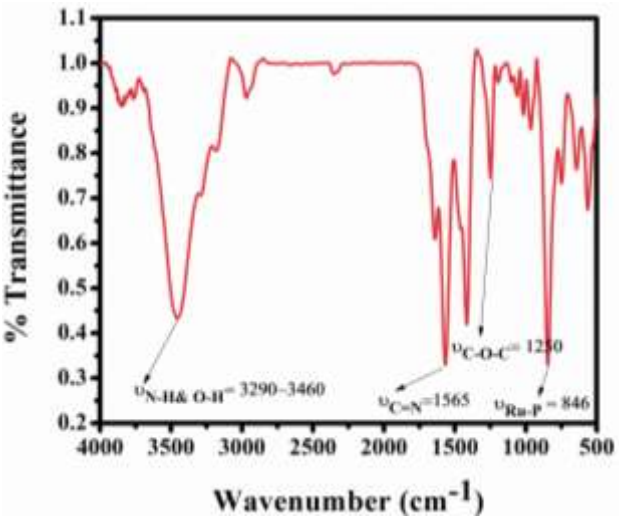

***Figure 4.18:** FT-IR spectrum of complex **3**.*

4.3.4 Elemental Analysis

Elemental analysis for ligand (**HL**) (%): Calc. for $C_{14}H_{12}N_2O_2$: C, 69.99; H, 5.03; N, 11.66; Found: C, 69.83; H, 5.11; N, 11.72.

Elemental analysis for complex **1** (%): Calc. for $C_{24}H_{25}ClN_2O_2Ru$: C, 56.52; H, 4.94; N, 5.49; Found: C, 56.45; H, 5.02; N, 5.52.

Elemental analysis for complex **2** (%): Calc. for $C_{42}H_{40}F_6N_2O_2P_2Ru$: C, 57.21; H, 4.57; N, 3.18; Found: C, 57.08; H, 4.62; N, 3.21.

Elemental analysis for complex **3** (%): Calc. for $C_{30}H_{37}F_6N_5O_2P_2Ru$: C, 46.39; H, 4.80; N, 9.02; Found: C, 46.43; H, 4.72; N, 8.96.

4.3.5 UV Spectra

The UV-Vis spectra (Figure 4.19) shows that both ligand (**HL**) and the complexes **1-3** produce a peak in the region of 220-250 nm which corresponds to π→π* transition along with another one in the 300-335 nm region which is due to n → π* transitions.[31] Apart from this, only the complexes show an additional peak in the range of 350-400 nm which represents the MLCT transition[54]

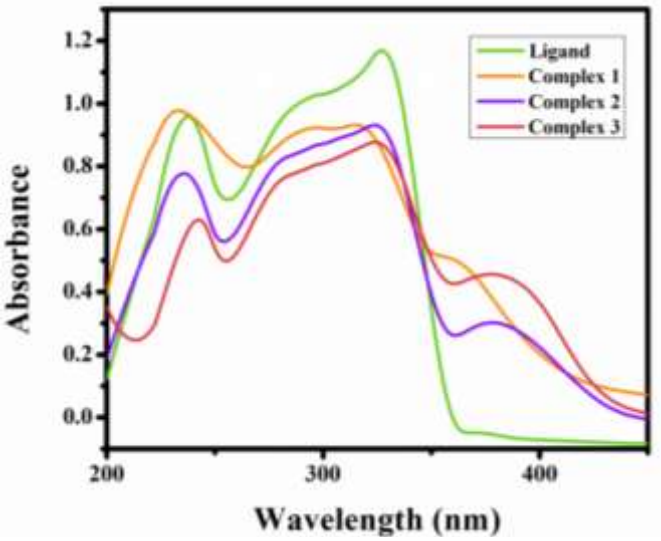

Figure 4.19: *UV- visible absorption spectra of ligand (**HL**) and complexes **1-3**.*

4.3.6 Fluorescence Spectra

As the complexes are found to be fluorescent in nature therefore to record the emission spectra, complexes **1-3** were excited at the wavelengths corresponding to the excitation wavelengths given in Table 4.1. Around 363 nm, the ligand (**HL**) shows the emission band which is found to be weaker than the corresponding ruthenium complexes. In case of the compounds **1-3**, emission bands are observed at 357 nm for complex **3**, at 358 nm for complex 2, and at 359 nm for complex **1** in increasing order of intensities (Figure 4.20). Furthermore, other higher intensity bands are observed at around 485 nm for all the compounds (Table 4.1) with the relative intensity of **3≈1**> **2**> **HL**.

Table 4.1: *Excitation and emission wavelengths of ligand (**HL**) and complexes **1-3**.*

Compound	UV-Vis (nm)	$\lambda_{excitation}$ (nm)	$\lambda_{emission}$ (nm)
Ligand (**HL**)	327, 238	327	363, 482
Complex **1**	357, 315, 233	315	359, 486
Complex **2**	378, 324, 236	324	358, 485
Complex **3**	377, 324, 243	324	357, 484

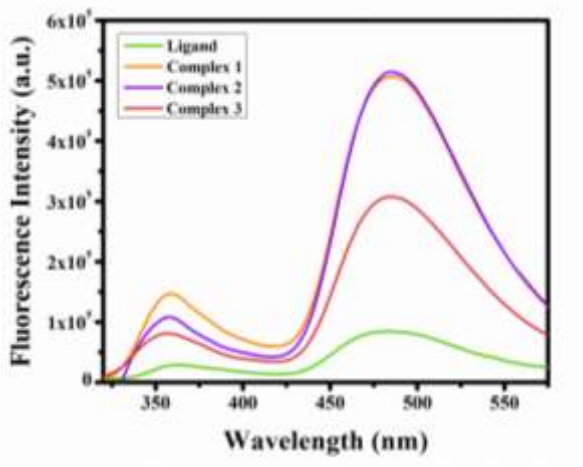

Figure 4.20: *Fluorescence spectra of ligand (**HL**) and complexes **1-3**.*

4.4 Stability Study of the Complexes

The synthesized complexes have been tested for their stability as they should not decompose in biological medium in order to function properly. A solution of 1% DMSO/PBS was taken and the complexes (0.1 mM) were dissolved in it after which their UV spectra were recorded at various time intervals ranging from 0-48 hours (Figure 4.21). It was observed that there is no noticeable change in the UV spectra peaks which confirms that the complexes maintain their stability in biological medium.

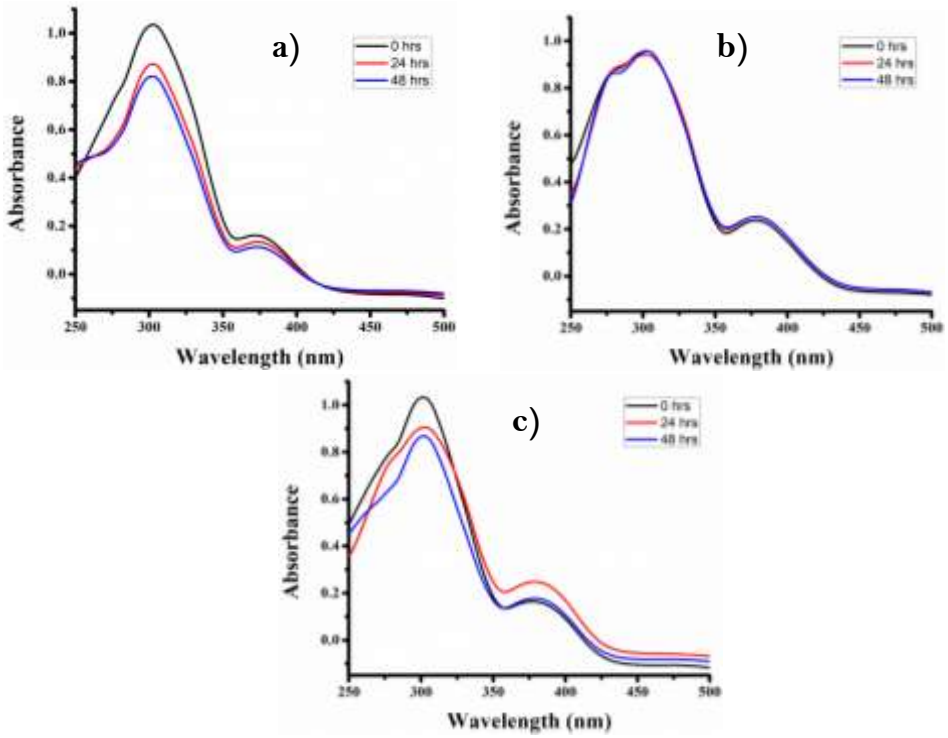

Figure 4.21*: Stability study of the (a) complex* ***1****, (b) complex* ***2****, and (c) complex* ***3*** *(in 1% DMSO in PBS Solution) using UV spectroscopy.*

4.5 Lipophilicity Study

An important parameter for metal based drugs is its lipophilicity as it sheds light on the potential extent of cellular uptake through cell membranes and on its ability to bind to proteins which is essential for transportation.[55] Lipophilicity expressed in terms of partition coefficient (log $P_{o/w}$) was determined through shake flask method by measuring the ratio of equilibrium concentration between the n-octanol (organic) phase and water (aqueous) phase. The coefficient was calculated using the optical density through UV spectroscopy and the results are presented in Table 4.2. As anticipated complex **2** which contains three hydrophobic phenyl rings as a part of PPh_3 group showed the highest log P value of 1.098 while complex **1** and **3** demonstrated lower lipophilicity.

Table 4.2: *Values of partition coefficients (log P) of complexes* ***1-3*** *in octanol/water.*

Compound	log $P_{o/w}$
Complex **1**	-0.853
Complex **2**	1.098
Complex **3**	-0.614

4.6 Protein Binding Study

4.6.1 Fluorescence Spectra

Serum albumin proteins help in the transportation of metallodrugs via blood to the targeted cells. Therefore it is very important to study whether the synthesized complexes can show sufficient binding with these proteins. Two such serum albumins used for the study are i) Bovine Serum Albumin or BSA and ii) Human Serum Albumin or HSA. The difference between BSA and HSA is that the former has two residues of tryptophan (Trp-134) and (Trp-212) whereas the latter contains only one (Trp-214).[56] In UV region, BSA/HSA emits fluorescence primarily due to this tryptophan residue. When BSA/HSA binds to other molecules, the fluorescence emitted due to tryptophan changes depending on the changes in the protein conformation and by studying this change in fluorescence the extent of complex binding with protein can be investigated.

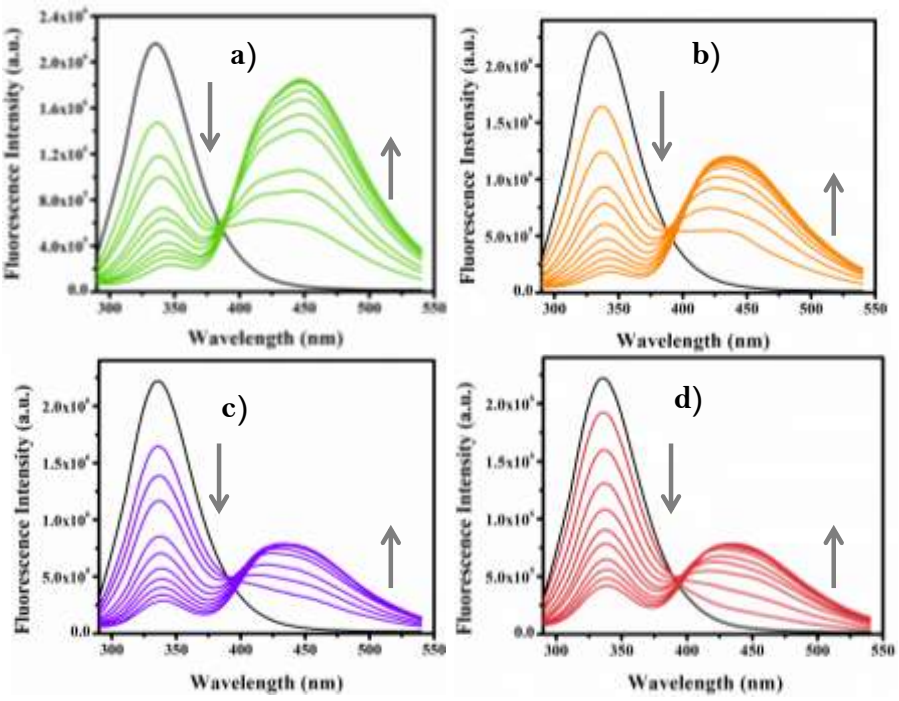

Figure 4.22: *Fluorometric titration spectra of BSA (10 μM) in buffer solution with (a) ligand (**HL**), (b) complex **1**, (c) complex **2**, and (d) complex **3** (2-20 μM) at 298 K.*

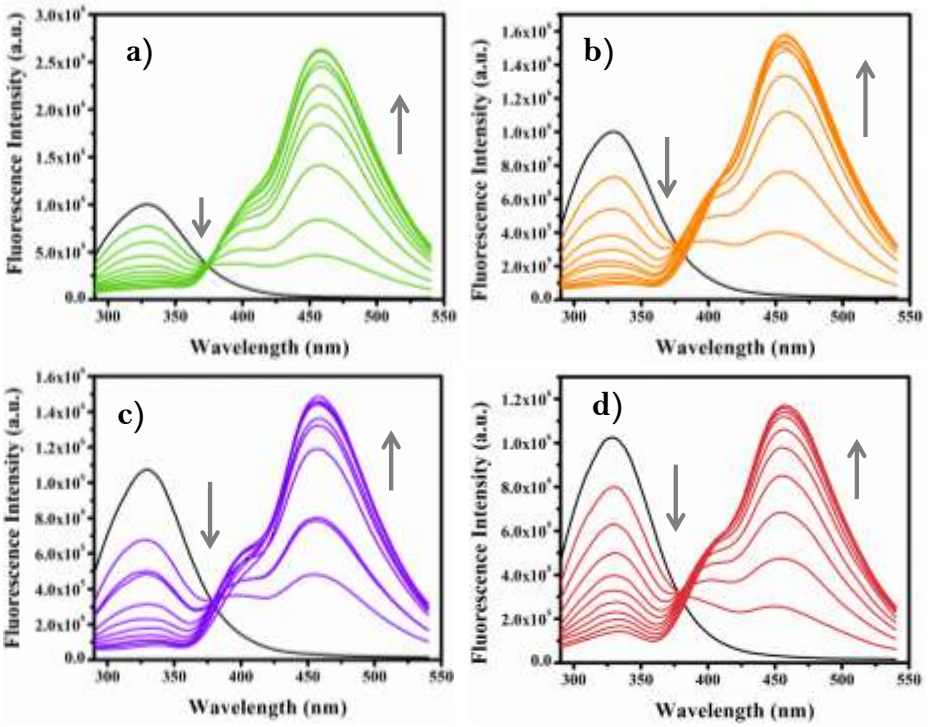

***Figure 4.23**: Fluorescence quenching spectra of HSA (10 μM) of (a) ligand (**HL**), (b) complex **1**, (c) complex **2**, and (d) complex **3** (2-20 μM) at 298 K.*

It was observed that as the concentration of the compounds increased (0-20 μM) in BSA/HSA solution the intensity of the corresponding peak at around 335 nm gradually decreases and a new peak gets slowly emerged at around 445 nm with the excitation wavelength of 280 nm (Figure 4.22, Figure 4.23). An explanation for this behavior is that the original emission due to the protein is getting quenched as it binds to the complex while the newer peak at longer wavelength is because of the inherent fluorescence of the complexes and the ligand respectively.

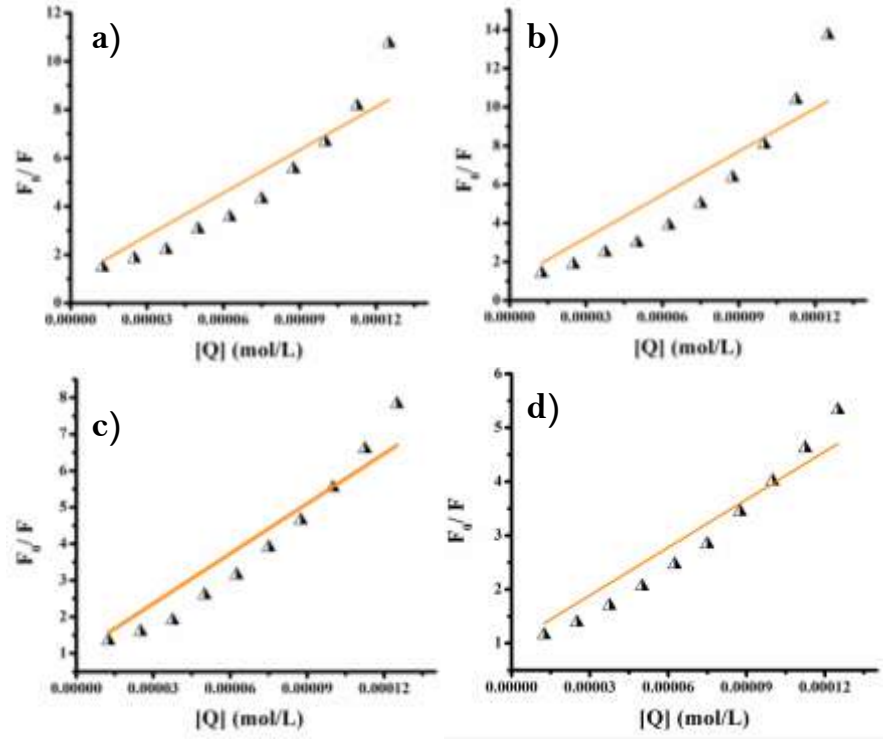

Figure 4.24: *Stern Volmer plots for the titration of BSA with (a) ligand (**HL**) , (b) complex **1**, (c) complex **2**, (d) complex **3**.*

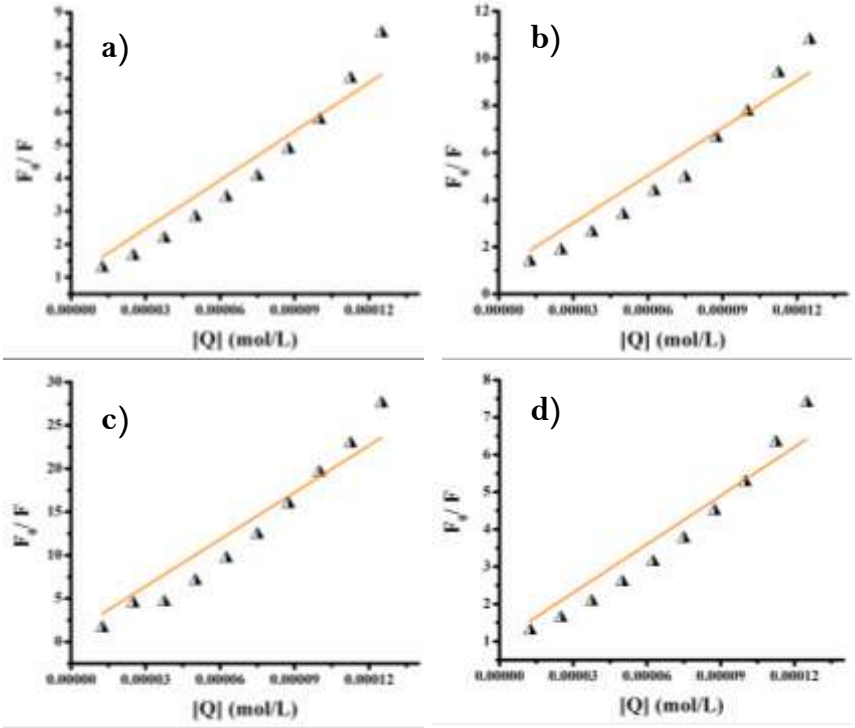

Figure 4.25: *Stern Volmer plots for the titration of HSA with (a) ligand (**HL**) , (b) complex **1**, (c) complex **2**, (d) complex **3**.*

Binding ability of the ligand (**HL**) and complexes **1-3** with BSA/HSA, was studied using various binding parameters which were calculated by the Stern Volmer equation (Figure 4.24, Figure 4.25) and Scatchard equation, the results of which are displayed in Table 4.3. It is evident that complex **2** with a k_q value of 2.9×10^{13} $M^{-1}s^{-1}$ and 1.1×10^{13} $M^{-1}s^{-1}$ for HSA and BSA respectively shows maximum binding with the proteins. This is probably due to an increased hydrophobic interaction between the protein non polar side chains and the p-cymene group and large phenyl groups of PPh_3 present in the complex **2**. Furthermore, the above mentioned high k_q value signifies an occurrence of static quenching.[31]

Table 4.3: *Various parameters to analyze the binding between proteins and the compounds from SV and Scatchard plots.*

Compound	**$K_{sv}(M^{-1})$**	**$K_q(M^{-1}s^{-1})$**	**$K_a(M^{-1})$**	**n**
		BSA		
Ligand (**HL**)	5.9×10^4	9.5×10^{12}	9.5×10^5	1.3
Complex **1**	4.6×10^4	7.4×10^{12}	1.1×10^6	1.35
Complex **2**	7.4×10^4	1.1×10^{13}	5.5×10^6	1.5
Complex **3**	2.9×10^4	4.7×10^{12}	1.9×10^6	1.45
		HSA		
Ligand (**HL**)	4.9×10^4	7.9×10^{12}	1.9×10^6	1.4
Complex **1**	6.7×10^4	1.1×10^{13}	3.6×10^6	1.43
Complex **2**	1.8×10^5	2.9×10^{13}	2.9×10^7	1.55
Complex **3**	4.3×10^4	6.7×10^{12}	1.1×10^6	1.35

4.7 DNA Binding Study

4.7.1 Absorption spectroscopy

UV spectroscopy is a very useful technique to conduct an investigation into the mode of interaction between the complexes and CT-DNA. Hypochromism on addition of complexes generally indicates intercalative mode of binding while hyperchromism indicates groove binding and other electrostatic interactions.[57] It can also suggest uncoiling of the DNA strand to some extent revealing more DNA bases.[58] Complexes **1**-**3** and ligand (**HL**) are titrated with CT-DNA in increasing amounts while the UV spectra is recorded in each step (Figure 4.26). For all the complexes, there is a noticeable increase in the absorption intensity, i.e. hyperchromism when compared to the absorption band of the free complex without CT-DNA. This confirms the groove binding nature or some other mode of electrostatic interaction through which our complexes show appreciable binding to the DNA.

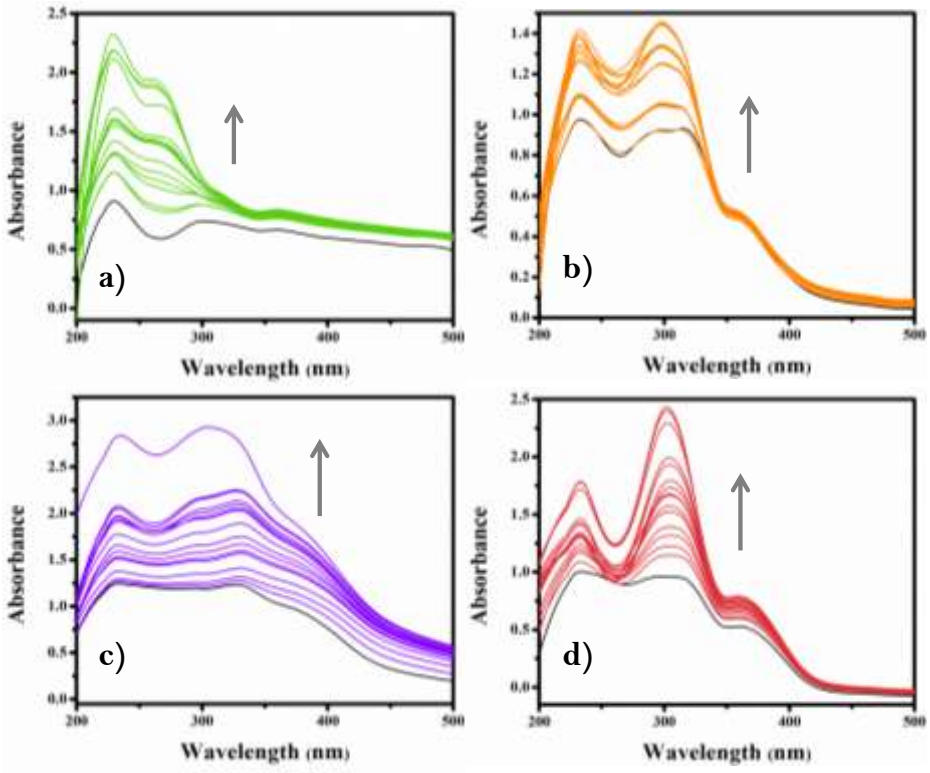

***Figure 4.26**: Absorption titration spectra of (a) ligand (**HL**), (b) complex **1**, (c) complex **2**, and (d) complex **3** with increasing concentrations of DNA.*

4.7.2 Emission Spectroscopy

DAPI is a fluorescent DNA stain that specifically attaches to the Adenine-Thymine base pairs of DNA minor groove. As a result, a competitive binding study was done via fluorometric titration by observing the changes in the emission intensity of DAPI-DNA adduct upon gradual addition of the compounds (0-100 μL) as the quencher.[31] It is observed that there is a distinct decrease in the intensity of fluorescence in all the cases (Figure 4.27) as the DAPI moiety gets displaced on increasing the compound concentration which is indicative of the minor groove binding nature of the complexes.

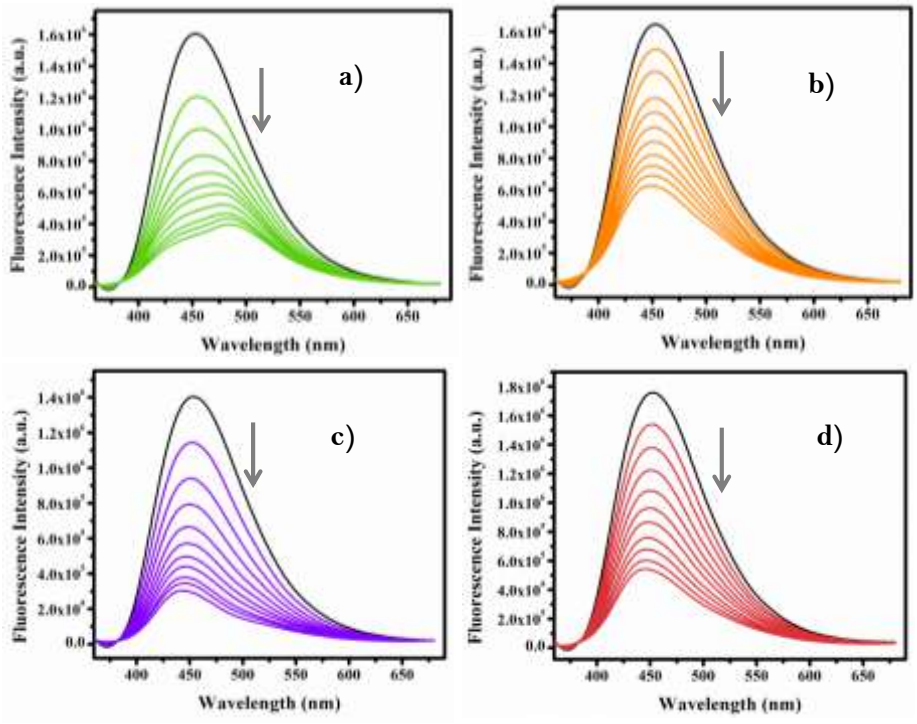

Figure 4.27: *Fluorescence quenching spectra of DAPI bound CT-DNA upon gradual addition of (a) ligand (**HL**), (b) complex **1**, (c) complex **2**, and (d) complex **3** as the quencher at 298 K.*

Stern-Volmer equation and Scatchard equation (Equations 2 and 3) have been utilized to calculate the binding parameters K_{SV}, K_q, K_a (Figure 4.28) the results of which have been shown in Table 4.4. High magnitudes of 10^4 of the calculated values of K_{SV} show beyond a doubt that a significant

amount of binding between the complexes and the DNA takes place where complex **2** exhibits the highest binding constants.

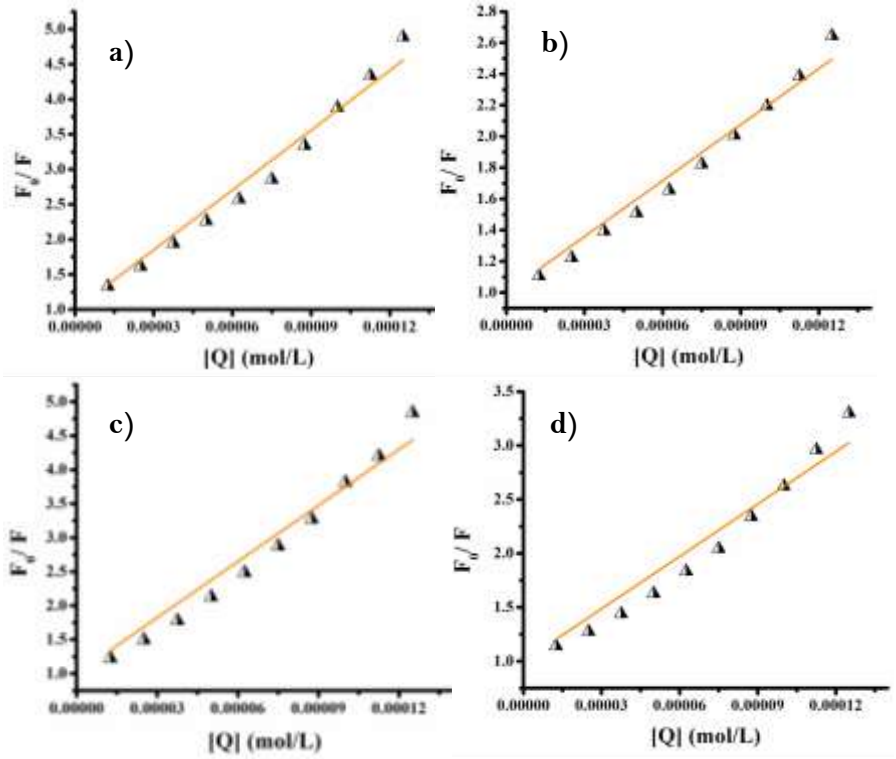

Figure 4.28: *Stern Volmer plots for the titration of DNA-DAPI with (a) ligand (**HL**) , (b) complex **1**, (c) complex **2**, (d) complex **3**.*

Table 4.4: *Binding parameters of DNA with complexes **1-3** and ligand (**HL**) analyzed from Stern Volmer and Scatchard plots.*

Compound	**$K_{sv}(M^{-1})$**	**$K_q(M^{-1}s^{-1})$**	**$K_a(M^{-1})$**	**n**
Ligand (**HL**)	2.8×10^4	1.3×10^{13}	5.1×10^4	1.07
Complex **1**	1.2×10^4	5.5×10^{12}	6.4×10^4	1.18
Complex **2**	2.7×10^4	1.2×10^{13}	2.1×10^5	1.22
Complex **3**	1.6×10^4	7.3×10^{12}	1.2×10^5	1.22

4.8 Catalytic Oxidation of NADH

Coenzymes NAD^+/NADH play a significant role in the control of enzymatic reactions and various aspects of cellular metabolism. The redox state of the cell controlled by the ratio between NAD^+/NADH, influences the activity of multiple cellular processes such as oxidative phosphorylation and the citric acid cycle[59]. So any disruption to this particular ratio can cause interference in regular metabolic activities of the cell.[60] Ru(II) aqua complexes have previously been reported to oxidize NADH to NAD^+ via catalytic transfer hydrogenation (TH) whereby the hydride from NADH migrates to form a Ru hydride adduct intermediate that further undergoes reaction to generate Reactive Oxygen Species (ROS).[31,61]

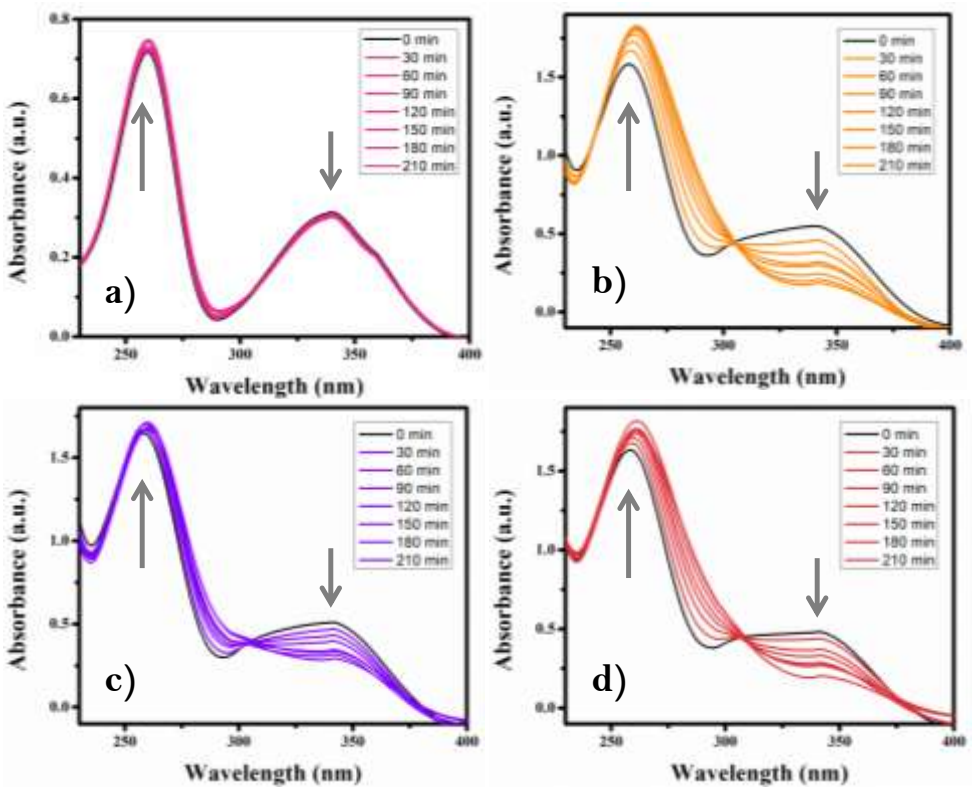

Figure 4.29: *UV-visible spectra of NADH (100 μM) on reaction with complexes* ***1–3*** *(5 μM): (a) only NADH, (b) complex* ***1****, (c) complex* ***2*** *and (d) complex* ***3****.*

The catalyzing ability of the synthesized compounds is hereby investigated using UV spectroscopy. In a solution of 90% H_2O + 10% MeOH, 100 μM NADH was incubated with complexes **1-3** (5 μM) while observing the peak at 339 nm, characteristic of NADH at various intervals of time. A gradual decrease in the aforementioned peak signified the oxidative transformation of NADH to NAD^+ while the control containing only a NADH solution showed negligible spectral changes (Figure 4.29). Using the spectra obtained, the values of TON (turnover numbers) of the complexes **1**, **2**, and **3** were calculated to be 11.78, 7.05 and 9.04 respectively (Figure 4.30). Complex **1** displays the highest TON on account of presence of a labile Cl leaving group which improves the catalytic rate. Thus all the complexes possess the ability to catalyze the oxidation reaction of NADH, thereby inducing an oxidative stress in tumor cells leading to apoptosis.[32]

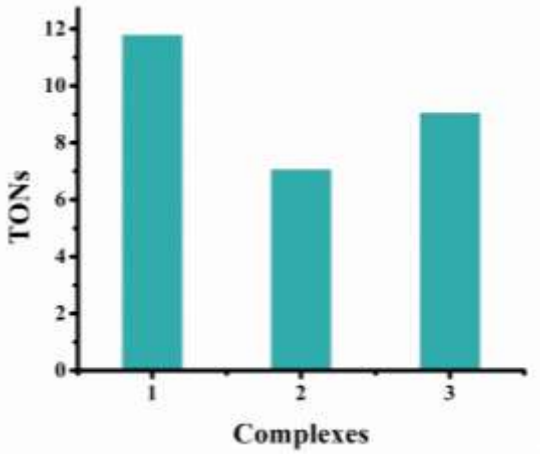

Figure 4.30*: Histogram displaying the turnover numbers of catalysis of NADH oxidation by the complexes **1-3**.*

4.9 *In Vitro* Cell Viability Assay

MTT colorimetric assay is utilized to analyze the cell viability following the treatment of cancer cells HeLa, MCF-7 and HEK 293 with the synthesized ruthenium(II) compounds. The assay is founded upon the reduction reaction of MTT or 3-[4,5-dimethylthiazole-2-yl]-2,5-diphenyltetrazolium bromide (soluble) which gets converted to formazan crystals (insoluble) by the enzymatic action of mitochondria in viable cells.[62] While the ligand showed mild anticancer activity, all the complexes **1**-**3** displayed strong cytotoxicity towards HeLa and MCF7 cancer cell lines as revealed by the cell viability curves at different concentrations of the compounds (Figure 4.31). Complex **2** containing the PPh_3 group exhibited the strongest potent ability to kill both HeLa and MCF7 cancer cells since it presents low IC_{50} values of 12.34 μM and 13.97 μM respectively (Table 4.5). The results obtained suggest that the increased efficacy is probably due to the large hydrophobic phenyl groups of PPh_3 that increases the lipophilic interactions with various biomolecules and allows an increase in the cellular uptake of the complexes through the non polar lipid bilayer cell membrane as evident from the cellular uptake study. On the contrary, the complexes displayed high IC_{50} values (>39 μM) when tested against normal HEK 293 cells thus demonstrating a good selectivity between malignant and non tumor cells. It is also noteworthy that in all the cases the toxicity increased many fold on complexation with Ru compared with the activity of the free ligand (**HL**).

Additionally, it is interesting to notice that there exists a direct relation between the lipophilicity of a complex and its cytotoxicity with complex **2** exhibiting the highest value of log P and simultaneously the highest antitumor activity. The above finding also agrees with literature where it has been found that charged cationic species show a higher cellular uptake which is often responsible for higher chemotherapeutic properties.[63]

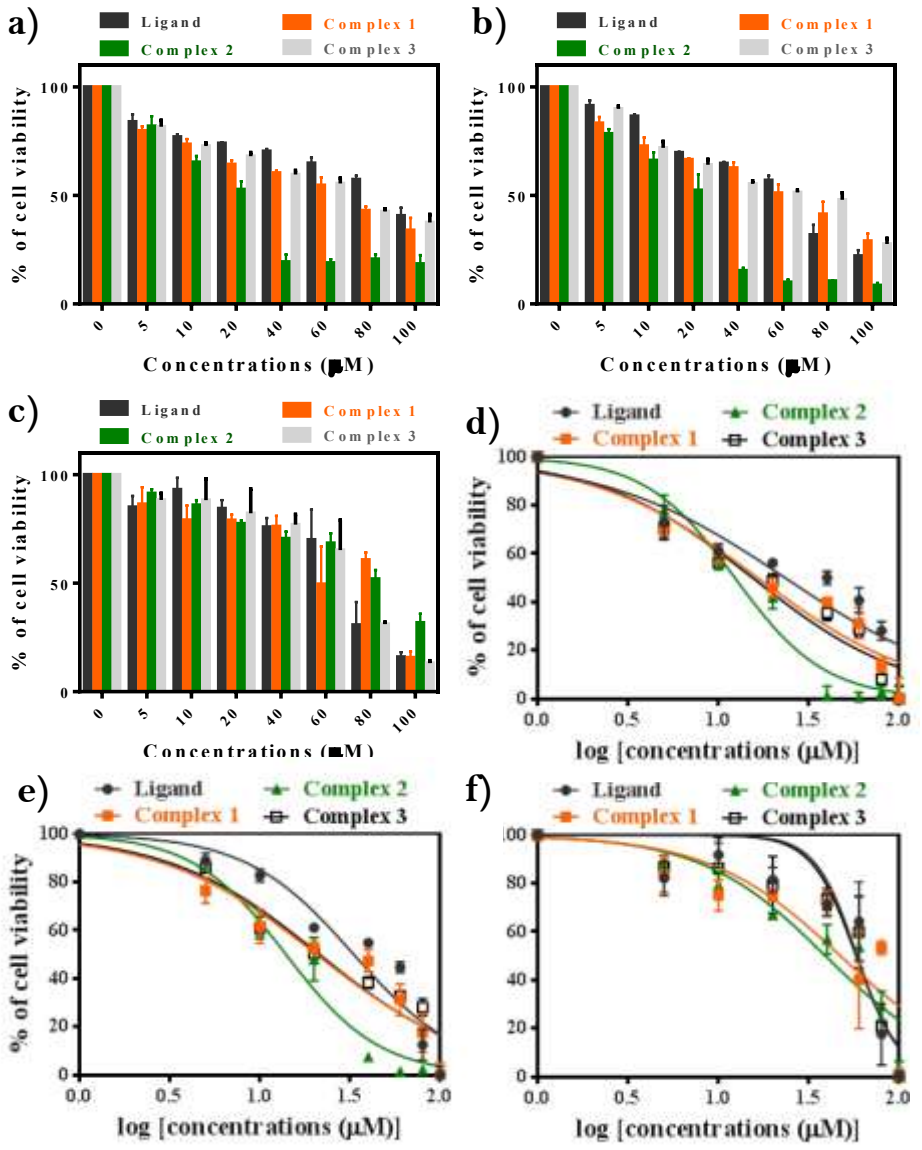

Figure 4.31: *Cell viability curve for ligand (**HL**) and complexes **1-3** against (a) HeLa, (b) MCF7 (cancer cell lines) and (c) HEK 293 (normal cell line) and normalized log of concentrations of the doses of ligand (**HL**) and complexes **1-3** against (d) HeLa, (e) MCF7 and (f) HEK 293.*

Table 4.5: *IC_{50} values obtained from MTT assay of the ligand (**HL**) and complexes **1-3** against cancer cell lines (HeLa and MCF- 7) along with a comparison with normal cell line (HEK 293).*

Compound	**IC_{50} Values (μM)**		
	HeLa	**MCF-7**	**HEK 293**
Ligand (**HL**)	23.46 ± 0.48	33.22 ± 0.42	58.60 ± 0.57
Complex **1**	16.52 ± 0.54	20.67 ± 0.72	47.36 ± 0.54
Complex **2**	12.34 ± 0.64	13.97 ± 0.46	39.16 ± 0.30
Complex **3**	15.50 ± 0.38	21.38 ± 0.40	57.82 ± 0.56

4.10 Apoptosis Study with Hoechst Staining Method

To investigate more into the effect of the complexes on cancer cells, the changes in cellular morphology were investigated under fluorescence microscope following a Hoechst 33258 staining of HeLa cells after treating them with the synthesized complexes **1-3** at their IC_{50} concentrations (Figure 4.32). The untreated cells displayed evenly and lightly stained structures with intact cell membranes. On the other hand, changes like swelling of the nucleus, cell rounding, chromatin fragmentation and rupturing of the cell membrane are observed for the treated cells which are characteristic of apoptosis in a cell[64], by confocal microscope.

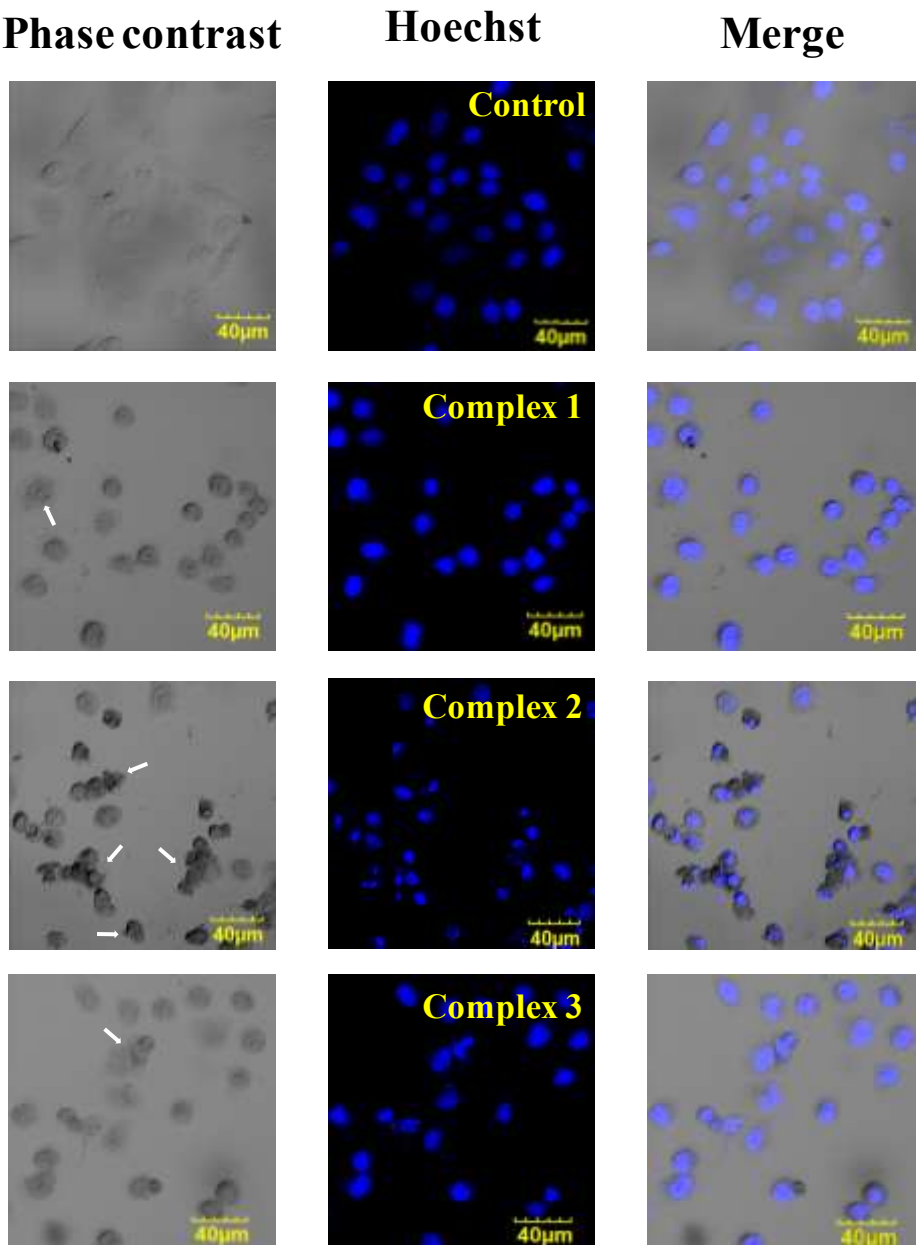

Figure 4.32: *Confocal image of treated HeLa cells with complexes* ***1-3*** *stained by Hoechst dye.*

CHAPTER 5 Conclusion and Future Scope

This work encompasses the synthesis of (i) [Ru(η^6-p-cym)(L)Cl] (ii) [Ru(η^6-p-cym)(L)PPh_3]PF_6 (iii) [Ru(η^6-p-cym)(L)(PTA)]PF_6 (where [L=2-(1H-benzo[d]imidazol-2-yl)-6-methoxyphenol] PPh_3 = triphenyl phosphine, PTA = 1,3,5-triaza-7-phosphaadamantane, p-cym = p-cymene). The composition and structure has been confirmed by various spectroscopic methods like MS, IR, NMR and UV spectroscopy. Adequate binding between the complexes with serum albumin proteins and CT-DNA was observed by fluorometric titrations while hyperchromism in the UV spectra of the complexes interacting with DNA revealed a groove binding mode of interaction. Additionally, all the synthesized compounds were found to be stable in biological medium and possessing the ability to catalyze the oxidation of NADH to NAD^+, thereby causing an enhanced production of ROS. Lipophilicity study was conducted via shake flask method to analyze the hydrophobicity of the complexes. The anticancer potential of the compounds was verified and quantified through an MTT assay against HeLa and MCF-7 (tumor cell lines) and HEK 293 (healthy cell line), with complex **2** showing the highest activity exclusively towards the malignant cells. Lastly, morphological changes detected under a fluorescence microscope following a treatment of tumor cells with the complexes and Hoechst stain confirmed apoptosis in the cells.

The results obtained in this study imply that the above synthesized complexes have the potential to be promising candidates in chemotherapeutics with further future studies. *In vivo* studies might be carried out in zebrafish embryo to predict the effect of the drugs on humans. Further, the complexes may be investigated for additional cellular targets like the mitochondria of the cell, enzymes like thioredoxin reductase, and certain cellular proteins, especially protein kinases. Lastly, in this work, the complexes were tested for only two cancer cell lines,

HeLa and MCF-7. Thus their cytotoxicity can be further explored against other cisplatin resistant cancer cell lines like human non-small cell lung carcinoma (NSCLC) cell line, A549 and human ovarian cancer cell line, A2780.

REFERENCES

(1) *Cancer Statistics - National Cancer Institute*. https://www.cancer.gov/about-cancer/understanding/statistics

(2) *What Is Cancer? - National Cancer Institute*. https://www.cancer.gov/about-cancer/understanding/what-is-cancer

(3) Frezza, M.; Hindo, S.; Chen, D.; Davenport, A.; Schmitt, S.; Tomco, D.; Ping Dou, Q. Novel Metals and Metal Complexes as Platforms for Cancer Therapy. *Curr. Pharm. Des.* **2010**, *16* (16), 1813–1825.

(4) Mjos, K. D.; Orvig, C. Metallodrugs in Medicinal Inorganic Chemistry. *Chem. Rev.* **2014**, *114* (8), 4540–4563.

(5) Cepeda, V.; Fuertes, M. A.; Castilla, J.; Alonso, C.; Quevedo, C.; Perez, J. M. Biochemical Mechanisms of Cisplatin Cytotoxicity. *Anti-Cancer Agents Med. Chem.- Anti-Cancer Agents* **2007**, *7* (1), 3–18.

(6) Ndagi, U.; Mhlongo, N.; Soliman, M. Metal Complexes in Cancer Therapy – an Update from Drug Design Perspective. *Drug Des. Devel. Ther.* **2017**, *Volume11*, 599–616.

(7) Galluzzi, L.; Senovilla, L.; Vitale, I.; Michels, J.; Martins, I.; Kepp, O.; Castedo, M.; Kroemer, G. Molecular Mechanisms of Cisplatin Resistance. *Oncogene* **2012**, *31* (15), 1869–1883.

(8) van Rijt, S. H.; Sadler, P. J. Current Applications and Future Potential for Bioinorganic Chemistry in the Development of Anticancer Drugs. *Drug Discov. Today* **2009**, *14* (23), 1089–1097.

(9) Chen, D.; Milacic, V.; Frezza, M.; Dou, Q. Metal Complexes, Their Cellular Targets and Potential for Cancer Therapy. *Curr. Pharm. Des.* **2009**, *15* (7), 777–791.

(10) Florea, A.-M.; Büsselberg, D. Cisplatin as an Anti-Tumor Drug: Cellular Mechanisms of Activity, Drug Resistance and Induced Side Effects. *Cancers* **2011**, *3* (1), 1351–1371.

(11) Ghosh, S. Cisplatin: The First Metal Based Anticancer Drug. *Bioorganic Chem.* **2019**, *88*, 102925.

(12) Kartalou, M.; Essigmann, J. M. Mechanisms of Resistance to Cisplatin. *Mutat. Res. Mol. Mech. Mutagen.* **2001**, *478* (1), 23–43.

(13) Lee, S. Y.; Kim, C. Y.; Nam, T.-G. Ruthenium Complexes as Anticancer Agents: A Brief History and Perspectives. *Drug Des. Devel. Ther.* **2020**, *Volume 14*, 5375–5392.

(14) Prabaharan, R.; Rengan, R.; Umapathy, D.; Arockiam, A. J. V.; Małecki, J. G. Assessment of Antiproliferative Activity of New Half-Sandwich Arene Ru (II) Furylbenzhydrazone Complexes. *Appl. Organomet. Chem.* **2022**, *36* (2), e6512.

(15) Antonarakis, E. S.; Emadi, A. Ruthenium-Based Chemotherapeutics: Are They Ready for Prime Time? *Cancer Chemother. Pharmacol.*

(16) Bergamo, A.; Gaiddon, C.; Schellens, J. H. M.; Beijnen, J. H.; Sava, G. Approaching Tumour Therapy beyond Platinum Drugs: Status of the Art and Perspectives of Ruthenium Drug Candidates. *J. Inorg.*

(17) Zeng, L.; Gupta, P.; Chen, Y.; Wang, E.; Ji, L.; Chao, H.; Chen, Z.-S. The Development of Anticancer Ruthenium(II) Complexes: From Single Molecule Compounds to Nanomaterials. *Chem. Soc. Rev.* **2017**, *46* (19), 5771–5804.

(18) Chen, H.; Parkinson, J. A.; Morris, R. E.; Sadler, P. J. Highly Selective Binding of Organometallic Ruthenium Ethylenediamine Complexes to Nucleic Acids: Novel Recognition Mechanisms. *J. Am. Chem. Soc.* **2003**, *125* (1), 173–186.

(19) Melchart, M.; Sadler, P. J. Ruthenium Arene Anticancer Complexes. In *Bioorganometallics*; Jaouen, G., Ed.; Wiley-VCH Verlag GmbH & Co. KGaA: Weinheim, FRG, 2006; pp 39–64.

(20) Dadci, L.; Elias, H.; Frey, U.; Hoernig, A.; Koelle, U.; Merbach, A. E.; Paulus, H.; Schneider, J. S. ..Pi.-Arene Aqua Complexes of Cobalt, Rhodium, Iridium, and Ruthenium: Preparation, Structure, and Kinetics of Water Exchange and Water Substitution. *Inorg. Chem.* **1995**, *34* (1), 306–315.

(21) Hung, Y.; Kung, W.-J.; Taube, H. Aquo Chemistry of Monoarene Complexes of Osmium(II) and Ruthenium(II). *Inorg. Chem.* **1981**, *20* (2), 457–463.

(22) Murray, B. S.; Babak, M. V.; Hartinger, C. G.; Dyson, P. J. The Development of RAPTA Compounds for the Treatment of Tumors. *Coord. Chem. Rev.* **2016**, *306*, 86–114.

(23) Prabaharan, R.; Rengan, R.; Umapathy, D.; Arockiam, A. J. V.; Małecki, J. G. Assessment of Antiproliferative Activity of New Half-Sandwich Arene Ru (II) Furylbenzhydrazone Complexes. *Appl. Organomet. Chem.* **2022**, *36* (2), e6512.

(24) Alessio, E. Thirty Years of the Drug Candidate NAMI-A and the Myths in the Field of Ruthenium Anticancer Compounds: A Personal Perspective. *Eur. J. Inorg. Chem.* **2017**, *2017* (12), 1549–1560.

(25) Alessio, E.; Messori, L. NAMI-A and KP1019/1339, Two Iconic Ruthenium Anticancer Drug Candidates Face-to-Face: A Case Story in Medicinal Inorganic Chemistry. *Molecules* **2019**, *24* (10), 1995.

(26) Hartinger, C. G.; Zorbas-Seifried, S.; Jakupec, M. A.; Kynast, B.; Zorbas, H.; Keppler, B. K. From Bench to Bedside – Preclinical and Early Clinical Development of the Anticancer Agent Indazolium Trans-[Tetrachlorobis(1H-Indazole)Ruthenate(III)] (KP1019 or FFC14A). *J. Inorg. Biochem.* **2006**, *100* (5), 891–904.

(27) Chatterjee, S.; Kundu, S.; Bhattacharyya, A.; Hartinger, C. G.; Dyson, P. J. The Ruthenium(II)–Arene Compound RAPTA-C Induces Apoptosis in EAC Cells through Mitochondrial and P53–JNK Pathways. *JBIC J. Biol. Inorg. Chem.* **2008**, *13* (7), 1149.

(28) Morris, R. E.; Aird, R. E.; del Socorro Murdoch, P.; Chen, H.; Cummings, J.; Hughes, N. D.; Parsons, S.; Parkin, A.; Boyd, G.; Jodrell, D. I.; Sadler, P. J. Inhibition of Cancer Cell Growth by Ruthenium(II) Arene Complexes. *J. Med. Chem.* **2001**, *44* (22), 3616–3621.

(29) Swaminathan, S.; Haribabu, J.; Mohamed Subarkhan, M. K.; Gayathri, D.; Balakrishnan, N.; Bhuvanesh, N.; Echeverria, C.; Karvembu, R. Impact of Aliphatic Acyl and Aromatic Thioamide Substituents on the Anticancer Activity of Ru(II)- *p* -Cymene Complexes with Acylthiourea Ligands— *in Vitro* and *in Vivo* Studies. *Dalton Trans.* **2021**, *50* (44), 16311–16325.

(30) Chen, J.; Zhang, Y.; Jie, X.; She, J.; Dongye, G.; Zhong, Y.; Deng, Y.; Wang, J.; Guo, B.; Chen, L. Ruthenium(II) Salicylate Complexes Inducing ROS-Mediated Apoptosis by Targeting Thioredoxin Reductase. *J. Inorg. Biochem.* **2019**, *193*, 112–123.

(31) Pragti; Kundu, B. K.; Upadhyay, S. N.; Sinha, N.; Ganguly, R.; Grabchev, I.; Pakhira, S.; Mukhopadhyay, S. Pyrene-Based Fluorescent Ru(II)-Arene Complexes for Significant Biological Applications: Catalytic Potential, DNA/Protein Binding, Two Photon Cell Imaging and *in Vitro* Cytotoxicity. *Dalton Trans.* **2022**, *51* (10), 3937–3953.

(32) Pragti; Kundu, B. K.; Sonkar, C.; Ganguly, R.; Mukhopadhyay, S. Modulation of Catalytic and Biomolecular Binding Properties of Ruthenium(II)-Arene Complexes with the Variation of Coligands for Selective Toxicity against Cancerous Cells. *Polyhedron* **2021**, *207*, 115379.

(33) Sonkar, C.; Malviya, N.; Sinha, N.; Mukherjee, A.; Pakhira, S.; Mukhopadhyay, S. Selective Anticancer Activities of Ruthenium(II)-Tetrazole Complexes and Their Mechanistic Insights. *BioMetals* **2021**, *34* (4), 795–812.

(34) Mandal, P.; Sonkar, C.; Dhankhar, S. S.; Nagaraja, C. M.; Mukhopadhyay, S. Ruthenium(II)-Arene Complexes Containing Ferrocenamide Ligands: Synthesis, Characterisation and Antiproliferative Activity against Cancer Cell Lines. *J. Organomet. Chem.* **2020**, *916*, 121247.

(35) Mandal, P.; Malviya, N.; Silva, M. F. C. G. da; Dhankhar, S. S.; Nagaraja, C. M.; Mobin, S. M.; Mukhopadhyay, S. Fine Tuning through Valence Bond Tautomerization of Ancillary Ligands in Ruthenium(II) Arene Complexes for Better Anticancer Activity and Enzyme Inhibition Properties. *Dalton Trans.* **2016**, *45* (48), 19277–19289.

(36) Mandal, P.; Kumar Kundu, B.; Vyas, K.; Sabu, V.; Helen, A.; Singh Dhankhar, S.; M. Nagaraja, C.; Bhattacherjee, D.; Pada Bhabak, K.; Mukhopadhyay, S. Ruthenium(II) Arene NSAID Complexes: Inhibition of Cyclooxygenase and Antiproliferative Activity against Cancer Cell Lines. *Dalton Trans.* **2018**, *47* (2), 517–527.

(37) Kilpin, K. J.; Clavel, C. M.; Edafe, F.; Dyson, P. J. Naphthalimide-Tagged Ruthenium–Arene Anticancer Complexes: Combining Coordination with Intercalation. *Organometallics* **2012**, *31* (20), 7031–7039.

(38) Gatti, A.; Habtemariam, A.; Romero-Canelón, I.; Song, J.-I.; Heer, B.; Clarkson, G. J.; Rogolino, D.; Sadler, P. J.; Carcelli, M. Half-Sandwich Arene Ruthenium(II) and Osmium(II) Thiosemicarbazone Complexes: Solution Behavior and Antiproliferative Activity. *Organometallics* **2018**, *37* (6), 891–899.

(39) Gaba, M.; Mohan, C. Development of Drugs Based on Imidazole and Benzimidazole Bioactive Heterocycles: Recent Advances and Future Directions. *Med. Chem. Res.* **2016**, *25* (2), 173–210.

(40) Boiani, M.; Gonzalez, M. Imidazole and Benzimidazole Derivatives as Chemotherapeutic Agents. *Mini-Rev. Med. Chem.* **2005**, *5* (4), 409–424.

(41) Yadav, G.; Ganguly, S. Structure Activity Relationship (SAR) Study of Benzimidazole Scaffold for Different Biological Activities: A Mini-Review. *Eur. J. Med. Chem.* **2015**, *97*, 419–443.

(42) Shah, K.; Chhabra, S.; Shrivastava, S. K.; Mishra, P. Benzimidazole: A Promising Pharmacophore. *Med. Chem. Res.* **2013**, *22* (11), 5077–5104.

(43) Elsayed, S. A.; Harrypersad, S.; Sahyon, H. A.; El-Magd, M. A.; Walsby, C. J. Ruthenium(II)/(III) DMSO-Based Complexes of 2-Aminophenyl Benzimidazole with In Vitro and In Vivo Anticancer Activity. *Molecules* **2020**, *25* (18), 4284.

(44) Yellol, J.; Pérez, S. A.; Buceta, A.; Yellol, G.; Donaire, A.; Szumlas, P.; Bednarski, P. J.; Makhloufi, G.; Janiak, C.; Espinosa, A.; Ruiz, J. Novel C,N-Cyclometalated Benzimidazole Ruthenium(II) and Iridium(III) Complexes as Antitumor and Antiangiogenic Agents: A Structure–Activity Relationship Study. *J. Med. Chem.* **2015**, *58* (18), 7310–7327.

(45) Li, L.; Wong, Y.-S.; Chen, T.; Fan, C.; Zheng, W. Ruthenium Complexes Containing Bis-Benzimidazole Derivatives as a New Class of Apoptosis Inducers. *Dalton Trans.* **2012**, *41* (4), 1138–1141.

(46) Martínez-Alonso, M.; Busto, N.; Jalón, F. A.; Manzano, B. R.; Leal, J. M.; Rodríguez, A. M.; García, B.; Espino, G. Derivation of Structure–Activity Relationships from the Anticancer Properties of Ruthenium(II) Arene Complexes with 2-Aryldiazole Ligands. *Inorg. Chem.* **2014**, *53* (20), 11274–11288.

(47) Anand, S.; Muthusamy, A.; Dineshkumar, S.; Kannapiran, N. Synthesis, Characterization, Optical, Thermal and Electrical Properties of Polybenzimidazoles. *J. Macromol. Sci. Part A* **2018**, *55* (3), 243–252.

(48) Lv, G.; Guo, L.; Qiu, L.; Yang, H.; Wang, T.; Liu, H.; Lin, J. Lipophilicity-Dependent Ruthenium N-Heterocyclic Carbene Complexes as Potential Anticancer Agents. *Dalton Trans.* **2015**, *44* (16), 7324–7331.

(49) Kumar Kundu, B.; Pragti; M. Mobin, S.; Mukhopadhyay, S. Studies on the Influence of the Nuclearity of Zinc(II) Hemi-Salen

Complexes on Some Pivotal Biological Applications. *Dalton Trans.* **2020**, *49* (43), 15481–15503.

(50) Das, M.; Kumar Kundu, B.; Tiwari, R.; Mandal, P.; Nayak, D.; Ganguly, R.; Mukhopadhyay, S. Investigation on Chemical Protease, Nuclease and Catecholase Activity of Two Copper Complexes with Flexidentate Schiff Base Ligands. *Inorganica Chim. Acta* **2018**, *469*, 111–122.

(51) Kumar Kundu, B.; Pragti; Biswas, S.; Mondal, A.; Mazumdar, S.; M. Mobin, S.; Mukhopadhyay, S. Unveiling the Urease like Intrinsic Catalytic Activities of Two Dinuclear Nickel Complexes towards the in Situ Syntheses of Aminocyanopyridines. *Dalton Trans.* **2021**, *50* (14), 4848–4858.

(52) Kundu, B. K.; Mandal, P.; Mukhopadhyay, B. G.; Tiwari, R.; Nayak, D.; Ganguly, R.; Mukhopadhyay, S. Substituent Dependent Sensing Behavior of Schiff Base Chemosensors in Detecting Zn2+and Al3+ Ions: Drug Sample Analysis and Living Cell Imaging. *Sens. Actuators B Chem.* **2019**, *282*, 347–358.

(53) Beurskens, P. T.; Cras, J. A.; Van der Linden, J. G. M. Preparation, Structure, and Properties of Bis(N,N-Di-n-Butyldithiocarbamato)Gold(III) Bromide and Bis(N,N-Di-n-Butyldithiocarbamato)Gold(III) Tetrabromoaurate(III). *Inorg. Chem.* **1970**, *9* (3), 475–479.

(54) Ramadan, R. M.; Elsheemy, W. M.; Hassan, N. S.; Aziz, A. A. A. Synthesis, Spectroscopic Characterization, Thermal Behaviour, in Vitro Antimicrobial and Anticancer Activities of Novel Ruthenium Tricarbonyl Complexes Containing Monodentate V-Shaped Schiff Bases. *Appl. Organomet. Chem.* **2018**, *32* (3), e4180.

(55) Richert, M.; Walczyk, M.; Janusz Cieślak, M.; Kaźmierczak-Barańska, J.; Królewska-Golińska, K.; Wrzeszcz, G.; Muzioł, T.; Biniak, S. Synthesis, X-Ray Structure, Physicochemical Properties and Anticancer Activity of Mer and Fac Ru(III) Triphenylphosphine

Complexes with a Benzothiazole Derivative as a Co-Ligand. *Dalton Trans.* **2019**, *48* (28), 10689–10702.

(56) Belatik, A.; Hotchandani, S.; Carpentier, R.; Tajmir-Riahi, H.-A. Locating the Binding Sites of Pb(II) Ion with Human and Bovine Serum Albumins. *PLoS ONE* **2012**, *7* (5), e36723.

(57) Szymańska, M.; Pospieszna-Markiewicz, I.; Mańka, M.; Insińska-Rak, M.; Dutkiewicz, G.; Patroniak, V.; Fik-Jaskółka, M. A. Synthesis and Spectroscopic Investigations of Schiff Base Ligand and Its Bimetallic Ag(I) Complex as DNA and BSA Binders. *Biomolecules* **2021**, *11* (10), 1449.

(58) Ramadevi, P.; Singh, R.; Jana, S. S.; Devkar, R.; Chakraborty, D. Ruthenium Complexes of Ferrocene Mannich Bases: DNA/BSA Interactions and Cytotoxicity against A549 Cell Line. *J. Photochem. Photobiol. Chem.* **2015**, *305*, 1–10.

(59) Balaban, R. S. Regulation of Oxidative Phosphorylation in the Mammalian Cell. *Am. J. Physiol.-Cell Physiol.* **1990**, *258* (3), C377–C389.

(60) Tyagi, K.; Dixit, T.; Venkatesh, V. Recent Advances in Catalytic Anticancer Drugs: Mechanistic Investigations and Future Prospects. *Inorganica Chim. Acta* **2022**, *533*, 120754.

(61) Betanzos-Lara, S.; Liu, Z.; Habtemariam, A.; Pizarro, A. M.; Qamar, B.; Sadler, P. J. Organometallic Ruthenium and Iridium Transfer-Hydrogenation Catalysts Using Coenzyme NADH as a Cofactor. *Angew. Chem.* **2012**, *124* (16), 3963–3966.

(62) van Meerloo, J.; Kaspers, G. J. L.; Cloos, J. Cell Sensitivity Assays: The MTT Assay. In *Cancer Cell Culture: Methods and Protocols*; Cree, I. A., Ed.; Methods in Molecular Biology; Humana Press: Totowa, NJ, 2011; pp 237–245.

(63) Mazuryk, O.; Magiera, K.; Rys, B.; Suzenet, F.; Kieda, C.; Brindell, M. Multifaceted Interplay between Lipophilicity, Protein Interaction and Luminescence Parameters of Non-Intercalative Ruthenium(II)

Polypyridyl Complexes Controlling Cellular Imaging and Cytotoxic Properties. *JBIC J. Biol. Inorg. Chem.* **2014**, *19* (8), 1305–1316.

(64) Tang, B.; Wan, D.; Lai, S.-H.; Yang, H.-H.; Zhang, C.; Wang, X.-Z.; Zeng, C.-C.; Liu, Y.-J. Design, Synthesis and Evaluation of Anticancer Activity of Ruthenium (II) Polypyridyl Complexes. *J. Inorg. Biochem.* **2017**, *173*, 93–104.